Are Large Core Radius Clusters Merging Systems?

NASA GRANT NAG5-1871

Annual Report #3 and Final Report
For the Period 15 February 1992 through 14 February 1997

Principal Investigator
Dr. William R. Forman

May 1997

Prepared for:

National Aeronautics and Space Administration
Goddard Space Flight Center
Greenbelt, Maryland 20771

Smithsonian Institution
Astrophysical Observatory
Cambridge, Massachusetts 02138

The Smithsonian Astrophysical Observatory
is a member of the
Harvard-Smithsonian Center for Astrophysics

The NASA Technical Officer for this grant is Dr. Robert Petre, NASA, Goddard Space Flight Center, Mailstop 662.0, Greenbelt, MD 20771.

1 Report for NAG5-1871

We have analyzed observations for two lensing clusters of galaxies – A1689 and A2218. Our investigations have explored the implications of their X-ray properties for mass determinations both in X-rays and through both weak and strong gravitational lensing. The work on these two clusters is summarized below and copies of the two papers submitted to the Astrophysical Journal and accepted for publication are attached.

2 The Gravitating Mass Of The X-Ray Bright Lensing Cluster A1689

Our analysis of A1689 combined ROSAT imaging along with Ginga and ASCA spectroscopy. Combining these data, we derived a range of acceptable potentials for A1689 assuming that the gas is in hydrostatic equilibrium and that non-thermal pressure support can be neglected. We confirmed that the faint optical arcs observed in A1689 lie at radii which are too large to be produced by a simple smooth spherical potential, consistent with the X-ray data. Furthermore, the X-ray data imply total gravitating masses which are smaller than the masses derived from the analysis of arclets at all radii.

Although the X-ray observations show no evidence of substructure, the cluster velocity dispersion is too large to be due to a single cluster with the gas temperature and mass measured through the X-ray observations, under the assumptions of hydrostatic equilibrium. In addition, the velocity differences among the three brightest galaxies in the cluster core are unusually large. The distribution of galaxy radial velocities suggests the superposition of one or more subclusters directly along the line-of-sight to the primary A1689 cluster.

We conclude that the discrepancy for A1689 between the X-ray and gravitational lens mass determinations may not require non-thermal pressure support or gas flows. All the data taken together are consistent with either (1) the superposition of one or more subclusters directly along the line-of-sight to the primary A1689 cluster, (2) a single superposition combined with strong ellipticity or aligned substructure in the cluster core or (3) a breakdown in the underlying assumptions of hydrostatic equilibrium and thermal support of a single phase gas. Thus, if, as the optical kinematic data suggest, we are viewing A1689 along a direction containing several subcondensations, then the gas can be in hydrostatic equilibrium supported primarily by its thermal pressure.

3 A2218: X-Ray Lensing, Merger, Or Both?

Comparison of the high resolution X-ray image of A2218 obtained with the ROSAT HRI with the optical HST image shows several interesting correlations. The X-ray emission within a $1'$ radius core is resolved into several components; the central dominant galaxy does not coincide with either of them or the emission centroid. The major X-ray peak is an elongated feature

that lies between the two mass concentrations known from the optical lensing analysis, and coincides with optical arcs at $r \simeq 20''$ from the cD galaxy. We speculate that this may be lensed X-ray emission, for example (but not necessarily) of the same object lensed in the optical. Alternatively, this feature may be a merger shock, or a gas trail of an infalling subgroup. Two other X-ray enhancements are close to the two major mass concentrations. Both lensing and a merger are likely.

Previous X-ray derivations of the A2218 mass used a β-model fit to the data with angular resolution that blurred the features mentioned above into a broad constant core. As the HRI data show, such a core does not exist. Because of this, under certain assumptions and using only the improved imaging data, the hydrostatic estimate of the projected mass within the lensing radius can in principle be increased by a factor of ~ 1.4 (and the mass within a sphere of the same radius by a factor of 2.6) compared to previous analyses. However, for a merging cluster, the hydrostatic analysis is generally inapplicable. Most other lensing clusters are more distant than A2218 and obtaining adequate X-ray images and temperature maps of them is even more difficult. Together with the likely overestimation of mass by the lensing analysis (as in the simulations), oversimplification of the gas density and temperature models resulting from inadequate resolution may account for the lensing/X-ray mass discrepancy as suggested for A2218.

SUBMITTED TO *The Astrophysical Journal*
Preprint typeset using LaTeX style emulateapj

THE GRAVITATING MASS OF THE X-RAY BRIGHT LENSING CLUSTER A1689

S.DAINES[1], C. JONES, W.FORMAN
Center for Astrophysics, 60 Garden St., Cambridge, MA 02138
AND
J. A. TYSON
Bell Laboratories, Lucent Technologies, 700 Mountain Ave., Murray Hill, NJ 07974

submitted to The Astrophysical Journal

ABSTRACT

We present the analysis of a ROSAT PSPC observation of the X-ray luminous cluster of galaxies Abell 1689. Using the X-ray surface brightness distribution from the PSPC and mean temperatures from Ginga and ASCA, we derive a range of acceptable potentials for A1689 assuming that the gas is in hydrostatic equilibrium and that non-thermal pressure support can be neglected. We confirm that the faint optical arcs observed in A1689 lie at radii which are too large to be produced by a simple smooth spherical potential, consistent with the X-ray data. Furthermore, the X-ray data imply total gravitating masses which are smaller than the masses derived from the analysis of arclets at all radii.

Although the X-ray observations show no evidence of substructure, the cluster velocity dispersion is too large to be due to a single cluster with the gas temperature and mass measured through the X-ray observations, under the assumptions of hydrostatic equilibrium. In addition, the velocity differences among the three brightest galaxies in the cluster core are unusually large. In particular, while the brightest galaxy has a velocity nearly equal to the cluster mean while the other two have relative velocities of +4767 km $\sec^{-1}$ and -2686 km $\sec^{-1}$. The distribution of galaxy radial velocities suggests the superposition of one or more subclusters directly along the line-of-sight to the primary A1689 cluster.

We conclude that the discrepancy for A1689 between the X-ray and gravitational lens mass determinations may not require non-thermal pressure support or gas flows. All the data taken together are consistent with either (1) the superposition of one or more subclusters directly along the line-of-sight to the primary A1689 cluster, (2) a single superposition combined with strong ellipticity or aligned substructure in the cluster core or (3) a breakdown in the underlying assumptions of hydrostatic equilibrium and thermal support of a single phase gas. Thus, if, as the optical kinematic data suggest, we are viewing A1689 along a direction containing several subcondensations, then the gas can be in hydrostatic equilibrium supported primarily by its thermal pressure.

We also find that the cooling flow region in the cluster core is well resolved by the PSPC. Spectral fitting of the inner $1'$ shows emission from gas cooler than the average temperature, and consistent with a massive cooling flow of $\dot{M} \approx 500\,\mathrm{M}_\odot\ \mathrm{yr}^{-1}$, in agreement with the mass deposition rate found from a deprojection analysis of the imaging data.

Subject headings: Cosmology: Dark Matter – Galaxies: Clusters: Individual (Abell 1689) – Cosmology: Gravitational Lensing – X-rays: Sources – Galaxies: Cooling Flows

1. INTRODUCTION

Arcs and arclets in the cores of galaxy clusters are highly magnified, gravitationally lensed images of faint background galaxies (Lynds & Petrosian 1989, Soucail et al. 1988). In a smooth potential, the large arcs constrain the projected mass interior to the critical radius of the cluster. Arclets allow a more complete view of the cluster structure and can be used to define the cluster potential over large radii (e.g., Tyson, Valdes & Wenk 1990; Smail et al. 1994; Squires et al. 1996a; Squires et al. 1996b; see Mellier et al. 1996 for a recent review). The cluster potential can be measured through X-ray imaging and spectral observations, and through optical measurements of the galaxy distribution and velocities. X-ray observations of the cluster gas temperature and density profiles can be used through the hydrostatic equation to determine the total mass distribution (e.g., Bahcall and Sarazin 1977; Mathews 1978; Sarazin 1988). Through the standard virial theorem, cluster velocity dispersions also determine the cluster mass. Thus we have three different and independent ways of measuring the cluster mass. In principle, comparison of the different mass determinations provides fundamental insights into the structure and dynamics of the cluster and the physical state of the intracluster gas.

Each of these three methods is affected in different ways both by the shape of the potential relative to the line-of-sight, by substructure in the cluster, and by violations of the assumptions underlying the mass determinations. Optical velocity dispersion measurements are susceptible to contamination along the line-of-sight and frequently overestimate the cluster mass (and, due to the limited number of galaxies, generally provide little information on the mass distribution near the cluster core). Mapping the tangential distortion of faint background galaxies due to lensing in the cluster potential is a direct measure of the surface mass density out to large radii. Detailed modelling, and the statistics of the occurrence, of lensed giant arcs gives information on the mass distribution, shape and substructure of the

[1]Presently at the University of California, Berkeley

potential near the cluster core. However, as Bartelmann (1995) has shown, mass determinations from giant lensed arcs can overestimate the cluster mass if substructure is present. This bias is avoided in weak/strong lensing studies covering a wide radius range. With sufficient spatial resolution, X-ray observations often can distinguish the cluster substructure. However, in cluster cores with cooling flows, the complicated temperature structure hinders the determination of the mass distribution with the presently available X-ray observations. Current X-ray observations also limit the precision and spatial resolution to which the gas temperature profile can be determined, particularly for the hottest clusters. Lastly, the assumption of hydrostatic equilibrium with negligible non-thermal pressure support may not be valid (Miralda-Escude & Babul 1995; Loeb & Mao 1994), although as we argue in section 3.3, the effects of bulk flows or magnetic fields are not large enough to explain the mass discrepancies found for A1689 from X-ray and lensing analysis.

The relatively recent capabilities of both X-ray observations and the analysis of giant arcs and arclets to determine the mass distribution in clusters has led several investigators to compare the inferred cluster properties. One constraint on the central concentration comes from the observed arc widths or upper limits. From such a study of giant luminous arcs in six clusters, Hammer (1991) found that most of the lensing clusters must have a (total) mass distribution more compact than their X-ray gas density. Miralda-Escude & Babul (1995) used the radius of observed arcs (which are near the Einstein radius) to constrain the total mass within this radius and thereby compare the inferred and measured intracluster gas temperatures. They studied the three clusters A2218, A1689, and A2163. For A1689 and A2218, they found that the central cluster mass required to produce the observed arcs was a few times higher than expected based on the gas temperature of the ICM, and suggested that this may imply a non-thermal source of gas pressure. Loeb & Mao (1994) showed that in the core of A2218 the X-ray inferred gravitating mass was 2.5 times smaller than that required to produce the observed arcs. They suggested that magnetic fields and turbulence could play a significant role in providing pressure support to the X-ray emitting gas, thus causing X-ray mass measurements to be underestimates. However, since these first studies, more detailed analysis of these systems as well as the study of other clusters has often led to the conclusion that consistent mass models can be derived if multi-component models are used. For example, for A2218, Squires et al. (1995) and Kneib et al. (1995) showed that a cluster model comprised of two subclusters centered on the two bright galaxies reproduces the giant arcs and yields mass estimates from weak lensing which are consistent, for radii larger than 200 kpc, with those derived from X-ray observations under the hystrostatic assumption. Recently, for the cluster PKS0745, Allen et al. (1996) also found agreement between the mass derived from X-rays and that inferred from the giant arc. A1689 remains one of the clusters with no apparent substructure in its X-ray morphology, but with a large discrepancy in mass estimates. In particular, Tyson and Fischer (1995) derived the mass profile using the faint arclets detected in deep images and found that the projected masses are more than a factor of two larger than those calculated from the X-ray data, under the standard assumptions.

For A1689, the improved spatial resolution of the ROSAT PSPC, compared to that of the Einstein IPC which was used in earlier studies, as well as the spectral data from Ginga and ASCA, allows us to extend the past studies and make a detailed comparison of the cluster mass distribution constrained by the X-ray observations to that required to produce the observed arcs.

In this paper we present the analysis of our ROSAT PSPC observation of the cluster A1689. This is the 51st brightest, but the third most luminous, cluster in the X-ray flux limited sample of Edge et al. (1990). Tyson, Valdes, and Wenk (1990) detected many small, faint, weakly lensed arclets arising from gravitationally shear distorted galaxies behind the cluster. Although A1689 does not show bright, giant lensed arcs (the number density of bright background sources is low, so these are seen in only a small fraction of clusters), this cluster does contain several fainter, elongated arcs and numerous arclets. A1689 was selected for our study, as it has a relatively low redshift $z \approx 0.181$ for a lensing cluster, and previous X-ray observations with the Einstein IPC showed a smooth, relaxed morphology. In this paper, we use the surface brightness profile from the PSPC (angular resolution $\approx 0.25'$) and mean X-ray temperatures from Ginga and ASCA, to constrain the cluster mass distribution and thus to make a preliminary comparison with the position of the most distorted lensed arcs and the mass distribution inferred from the arclets.

The paper is organized as follows. In Section 2, we present the analysis of the ROSAT image. In Section 3, we derive a range of potentials for A1689 consistent with the X-ray measurements. In Section 4, we briefly review the galaxy radial velocity measurements and the cluster velocity dispersion and argue for the presence of substructure. Finally, in Section 5, we discuss our results and the lensing properties of the potentials we infer, from the X-ray data, for A1689.

We quote distance dependent quantities for a cosmology with $H_0 = 50\,\mathrm{km\,s^{-1}\ Mpc^{-1}}$, $q_0 = 0$, putting A1689 at an angular diameter distance of 0.85 Gpc for a redshift of $z = 0.181$ (1 arcmin at A1689 then corresponds to 247 kpc). The relation between the velocity dispersion of a potential of given angular scale, and surface density relative to the critical density, is independent of H_0 and at the redshifts considered is only weakly dependent on Ω.

2. A ROSAT PSPC OBSERVATION OF A1689

A1689 was observed with the ROSAT PSPC for 13,957s from 18 - 24 July 1992, giving $\approx$ 10,200 source counts within a radius of 8.5 arcmin (in ROSAT PI bins 40 - 200 corresponding to energies 0.4 to 2.0 keV). Extrapolating from the ROSAT band by assuming a nominal 9 keV thermal spectrum with a heavy element abundance of 0.29 solar and galactic column density $N_{\mathrm{H}} = 1.79 \times 10^{20}\,\mathrm{cm^{-2}}$ as derived from 21cm data (Stark et al. 1992), we find a 2 - 10 keV flux of $1.72 \times 10^{-11}\,\mathrm{erg\,cm^{-2}\,s^{-1}}$ and a source-frame 2 - 10 keV luminosity of $2.85 \times 10^{45}\,\mathrm{erg\,s^{-1}}$.

2.1. *Imaging analysis*

We show in Figure 1 a contour map of the adaptive-kernel smoothed PSPC image. In Figure 2, the inner 4′ is shown on an expanded scale with positions of galaxies with measured redshifts from Teague, Carter & Gray (1990; hereafter TCG), superimposed. The brightest cluster galaxy is TCG2. The larger lensed arcs from Tyson, Valdes & Wenk (1990; hereafter TVW), are indicated. The X-ray images show a rather symmetrical cluster with no apparent substructure.

Results of isophote fitting (Jedrzejewski 1987) to the adaptive-smoothed image of Figure 2 confirm that the X-ray image is close to circular, with ellipticity $\lesssim 0.1$ and centered within 4″ of the brightest cluster galaxy (TCG2). The coordinate system was derived by minimizing the residuals between maximum-likelihood X-ray positions of emission from three point sources, and their optical positions measured from the sky survey print (in two cases) and the quoted position of LBQS 1308-0111 (Hewett et al. 1991). This is related to the nominal ROSAT satellite pointing for this observation by a translation of the coordinates at the image center $\mathrm{RA} = \mathrm{RA}_{\mathrm{rosat}} + 5.8''$ and $\mathrm{Dec} = \mathrm{Dec}_{\mathrm{rosat}} + 7.3''$ (within the normal observation-to-observation scatter of ROSAT aspect solutions; L.David, private communication), and a rotation of the coordinate system by 0.285° counterclockwise (consistent with a known systematic error in the roll-angle of $0.185 \pm 0.099°$; ROSAT Status Report 67, US GOF).

The surface brightness profile of the cluster emission is shown in Figure 3. The cluster emission becomes comparable to the (mostly cosmic) background at a radius of 5 arcmin (in ROSAT PI channels 40 - 200, 0.4 - 2.0 keV). We are able to trace cluster emission out to ≈ 8.5 arcmin (comoving distance $2.1\, h_{50}^{-1}$ Mpc) where it is 15% of the background, and detectable at 2σ above the background in a 40″ radial bin.

The functional form

$$S(r) \propto (1 + (r/r_0)^2)^{-3\beta+1/2} \qquad (1)$$

(the 'isothermal β model', Cavaliere & Fusco-Femiano 1976) convolved with the instrument PSF (given by an energy-weighted sum over the function derived by Hasinger et al. 1993) and a flat background component provides an acceptable description of the X-ray surface brightness outside the innermost 50″ ($\chi^2 = 63.0$ for 50 degrees of freedom). We find a core radius for the X-ray gas of $r_0 = 1.13 \pm 0.12$ arcmin and slope parameter $\beta = 0.78 \pm 0.03$. For the purposes of the analysis of the mass distribution in Section 3.1, we also fit the surface brightness data of the whole cluster with a function of the form

$$S(r) = S_{\mathrm{bk}}(r/r_{\mathrm{bk}})^{-\alpha}(1 + (r/r_{\mathrm{bk}})^n)^{\alpha/n-\gamma/n} \qquad (2)$$

convolved with the PSF. We find a reasonable match to the data for values $1 \lesssim n \lesssim 2$. For $n = 1$ we obtain a best fit with $\chi^2 = 73.4$ for 54 degrees of freedom for break radius $r_{\mathrm{bk}} = 2.33^{+1.18}_{-0.70}$ arcmin, inner slope $\alpha = 0.53^{+0.12}_{-0.15}$, and outer slope $\gamma = 5.19^{+1.05}_{-0.65}$. The parameter values found for A1689 give a shape typical of nearby rich cooling flow clusters, with the logarithmic gradient of the surface brightness gradually flattening from -3.69 at a radius of 5′ to -0.90 at 0.2′, within the cooling radius. The convolved and unconvolved best fit models are shown superimposed on Figure 3 to indicate the effect of the instrumental point spread function. We confirm that the PSF significantly affects the derived surface brightness profile (and temperature solutions derived in Section 3.1) only within 0.25 arcmin of the cluster center.

A deprojection analysis (Fabian et al. 1981) of this imaging data shows a cooling flow mass deposition rate of $520 - 610\,\mathrm{M_\odot\,yr^{-1}}$ ($960 - 1090\,\mathrm{M_\odot\,yr^{-1}}$) and a cooling radius of $158 - 175$ kpc ($290 - 320$ kpc) for a cooling time equal to 1×10^{10} yr (2×10^{10} yr), for $H_0 = 50\,\mathrm{km\,s^{-1}\,Mpc^{-1}}$ and $q_0 = 0$. The ranges quoted are from the different mass models described in Section 3.1. Results for electron density, cooling time, and mass deposition rate are shown in Figure 4. These results are derived from a direct deprojection of the data, and give a lower limit on the electron density and an upper limit on the cooling time within the 15″ radius at which the effect of the point spread function is significant. The mass deposition rate is roughly twice that found by Arnaud (1988) from Einstein IPC data, reflecting the improved spatial resolution of the ROSAT PSPC which better resolves the cooling region within the cluster core.

2.2. *PSPC Spectral analysis*

The ROSAT PSPC has moderate spectral resolution of $\Delta E/E = 0.43(E/0.93\,\mathrm{keV})^{-0.5}$ with sensitivity in the range $0.1\,\mathrm{keV} \lesssim E \lesssim 2.3\,\mathrm{keV}$. The PSPC is capable of measuring the temperature of hot plasmas $kT \sim 10$ keV only from the small change in slope of the continuum, and therefore requires high statistical precision and accurate calibration to provide temperature measurements of hot clusters (*e.g.* A2256, Henry, Briel & Nulsen 1993). Conversely, it is highly sensitive to changes in spectral shape caused by Fe L-shell emission from cool components with $kT \sim 1$ keV and therefore able to detect cooler gas in the cores of such clusters.

To analyze the ROSAT PSPC spectrum, we divide the data into four annuli from $0' - 1'$, $1' - 3'$, $3' - 5'$, and $1' - 5'$. Collecting the 5650 background-subtracted counts from 1 to 5 arcmin (with background sources excluded) and fitting the spectrum from 0.11 to 2.24 keV with a single temperature thermal plasma model with abundance fixed at the ASCA value (0.29 solar, Section 2.3) we obtain fit parameters $kT = 10.7^{+11.1}_{-4.0}$ keV and $N_H = 1.49 \pm 0.17 \times 10^{20}\,\mathrm{cm^{-2}}$ with an acceptable $\chi^2 = 27.6$ for 29 degrees of freedom. Errors are quoted for $\Delta\chi^2 = 2.7$ corresponding to 90% confidence intervals on a single interesting parameter. The 90% confidence interval on the absorbing column density is slightly below the value from 21cm measurements of $1.79 \times 10^{20}\,\mathrm{cm^{-2}}$ (Stark et al. 1992). We also measured the best fit gas temperatures in the $1' - 3'$ and $3' - 5'$ to be 11.9 keV and 9.6 keV, respectively (with the hydrogen column density fixed at the best fit value from the $1' - 5'$ fit and the abundance set to the ASCA value). In computing the 90% confidence errors ($\Delta\chi^2 = 2.7$), upper bounds on the temperature could not be determined, but lower bounds for the $1' - 3'$ and $3' - 5'$ annuli were found to be 7.8 keV and 4.7 keV. Although the errors are large, there is no evidence for a temperature gradient. Had the outer temperature fallen significantly, the ROSAT PSPC would have been able to detect the temperature decrease.

The PSPC spectrum of the inner 1 arcmin shows the presence of cooler components, and is consistent with the presence of either a cooling flow of mass deposition rate consistent with that inferred from the deprojection analysis of the imaging data, or emission from a cooler single-phase model. A single-temperature plasma model with abundance fixed at 0.29 solar as determined by ASCA provides an acceptable description of the data ($\chi^2 = 20.2$ for 27 degrees of freedom) in the energy range 0.19 to 2.24 keV. The best fit temperature is $kT = 3.86^{+0.99}_{-0.67}$ keV and absorbing column density $N_{\mathrm{H}} = 2.13 \pm 0.14 \times 10^{20}\,\mathrm{cm^{-2}}$. We obtain an equally acceptable fit with a constant-pressure cooling-flow model (Johnstone et al. 1992, Mushotzky & Szymkowiak 1988), generated by co-adding single temperature plasma models with the emissivity appropriate to gas cooling at constant pressure from a given upper temperature. We fit a model consisting of a cooling flow component (with upper temperature and abundance fixed at the best fit ASCA values of 9 keV and 0.29 solar respectively) diluted by ambient cluster emission from a single tem-

perature model also with fixed temperature $kT = 9\,\mathrm{keV}$. Only the normalization of the two components, and the absorbing column density are left as free parameters. We then obtain $\chi^2 = 21.7$ for 27 degrees of freedom, $\dot{M} = 514 \pm 183\,\mathrm{M_\odot\ yr^{-1}}$, and $N_\mathrm{H} = 2.02 \pm 0.17 \times 10^{20}\,\mathrm{cm^{-2}}$.

Neither the single-phase nor the cooling-flow models fit the data in the lowest energy channels from 0.11 to 0.19 keV, and omitting these two channels reduces the χ^2 value by just over 20, to the values quoted. In both cases the model lies systematically above the data which could reflect absorption intrinsic to the inner part of the cooling flow (White et al. 1991, Allen et al. 1993). As a check on the overall consistency of the cooling-flow + isothermal model with the PSPC data, we fit this model also to the total spectrum from within 5′ and from 0.11 to 2.24 keV. We obtain $\chi^2 = 31.1$ for 29 degrees of freedom, with $\dot{M} = 490 \pm 209\,\mathrm{M_\odot\ yr^{-1}}$ and $N_\mathrm{H} = 1.84 \pm 0.09 \times 10^{20}\,\mathrm{cm^{-2}}$.

We find no significant difference in fit parameters between the two latest ROSAT PSPC calibrations from March 1992 and January 1993, (a test for systematic errors in the calibration) or between cooling flow models constructed from the Raymond-Smith and Mewe-Gronenschild-Kastra plasma codes (a test for sensitivity to assumed atomic parameters).

We conclude from spectral analysis of the PSPC data that cooler components are required within the central 1′, consistent either with a lower temperature, single-phase plasma, or with emission from a cooling distribution of temperatures. Although the central $0 - 1'$ region shows some evidence for X-ray absorption in excess of the galactic column density, the magnitude of the excess is much smaller than that found for some other cooling flow clusters which show large columns $\approx 10^{21}\ \mathrm{cm^{-2}}$ such as A478 (Allen et al. 1993). The PSPC data also do not rule out a contribution either from a point source or a cooler superposed subcluster to the spectrum of the cluster core.

2.3. *Ginga and ASCA Spectral Analysis*

To obtain broader spectral coverage above the ROSAT band and to determine the gas temperature accurately, we also analyzed both Ginga and ASCA spectra.

We jointly fit the Ginga and ROSAT spectra with the previously described cooling flow + single temperature model for the emission from A1689. One complication, arising from the large field of view of Ginga (FWHM 1° x 2°), is the presence of other sources. In particular, sources visible in the PSPC field of view, identified with the clusters MS 1306.7-0121 at $z = 0.088$ (Donahue et al. 1992) at 37′ off-axis and A1692 at 24′, contribute 30% of the PSPC count rate from A1689 (once corrected for vignetting and shadowing by the PSPC support structure) and lie at off-axis angles where the Ginga collimator has transmission of 50% and 60%. We approximate the effect of these less X-ray luminous clusters on the temperature of A1689 by including an additional 3 keV component in the Ginga fit. The Ginga background was determined from a nearby field observed close in time to the A1689 observation. Results are shown in Table 1. For comparison, a single-temperature fit to the Ginga data gives $7.85 \pm 0.5\,\mathrm{keV}$. The Ginga spectrum alone is insensitive to the presence of a cooling flow component, and adding this component into the fit as required by the PSPC increases the Ginga temperature by $\lesssim 0.4\,\mathrm{keV}$.

Note that for Ginga, a major uncertainty in determining the spectrum of a source with the count rate of A1689 (8 - 9 ct $\mathrm{s^{-1}}$) is the fluctuation in the cosmic Ginga background ($\approx 15\mathrm{ct\ s^{-1}}$ in the 2 - 10 keV band, with a 1σ variation of $\approx 0.8\mathrm{ct\ s^{-1}}$; Hayashida et al. 1989). To quantify the effect of this uncertainty on the spectral analysis, we analyzed the spectra using background determined from accumulated fields (Hayashida et al. 1989). As Table 1 shows, the second background method gives marginally hotter temperatures, but basically confirms the high temperature of A1689.

In principle, the ASCA observatory provides spatially resolved data for clusters of galaxies. However, two circumstances conspire to make spatially resolved analysis of A1689 unreliable at the present. First, A1689 is a moderately distant cluster, so the spatial resolution is limited. Second, the energy dependence of the point spread function, combined with the strong central surface brightness peak, makes analysis of A1689 data in multiple annuli unreliable. This is especially true because of A1689's high temperature (see Figure 4 of Ohashi 1994). An improved ASCA calibration will be needed before a detailed spatially resolved analysis of A1689 can be performed with confidence. Therefore, we analyze the data from A1689 as a single source using the standard screening and spectral extraction regions. We concentrate on the GIS which provides the most accurate estimate of the mean cluster temperature. In determining the GIS background, we selected the background files based on the rigidity of the GIS2 and GIS3 detectors independently.

We carried out several spectral fitting analyses for the GIS data from A1689. First, we fit the data in the 0.7-9.0 keV band, to a single temperature model. The resulting fit (see Table 1) gives a temperature of $8.98^{+0.45}_{-0.41}$ keV and an abundance of 0.29 ± 0.07 of solar. These are the values used in fitting the ROSAT spectra discussed previously. These GIS-derived values also are in good agreement with the fits from Ginga already discussed above. For the above fit, the column density was held fixed at the ROSAT-measured value. If the column density is allowed to be free, the temperature decreases by 0.5 keV and the column density rises to $4.2 \pm 2.1 \times 10^{20}\ \mathrm{cm^{-2}}$ which is higher than the galactic value.

The joint ROSAT and ASCA GIS fits provide broad coverage of the energy band and allow us to confirm the results of the Ginga/ROSAT fitting. We first fit the data to a single temperature model (with separate ASCA and ROSAT normalizations). This gave an acceptable fit (see Table 1) which shows little evidence for a cooling flow from the combined data set. However, we see the lower temperature component in the $0 - 1'$ annulus ROSAT spectrum. Continuing the analysis, we fit the ROSAT/ASCA spectra with a single temperature + cooling flow model, in which the cooling flow rate was fixed at $500\,\mathrm{M_\odot\ yr^{-1}}$. The resulting fit is significantly worse. The points that most deviate from the fit are the low energy points for ASCA. Excluding the lowest energy ASCA points, up to 1.5 keV, we obtain an acceptable value of χ^2 with a cooling flow rate consistent with that derived from the joint Ginga/ROSAT fits and the deprojection analysis (see Table 1). The low energy ASCA data tend to drive the fit toward one with less cooling gas. Figure 6 shows the resulting fit. The final resolution of the actual temperature profile and the detailed study of the cooling gas must await instruments of higher energy and spatial resolution.

The presence of a cooling flow requires that the ICM be multiphase at least within the cluster core (Thomas, Fabian and Nulsen 1987). As models for the multiphase structure are not completely constrained, this introduces an unavoidable uncertainty into the determination both of the gas density and mean thermal energy. The presence of cool components affects den-

sity determination from the PSPC surface brightness, as emission from gas cooling through 1 keV increases the PSPC counts per unit volume of a 9 keV constant-pressure cooling flow distribution by approximately a factor of 3 over a 9 keV single-phase gas (with the same pressure and the temperature equal to the upper temperature of the cooling flow). The cooling flow component contributes about 50% of the counts in our cooling flow + isothermal fit of the spectrum from the inner 1 arcmin. If the fractional contribution were independent of radius, a unit volume containing a fair sample of the multiphase gas is then 1/4 filled with cooler gas and 3/4 with single-phase gas, leading to a count rate per unit volume 1.5 times the single-phase value. A single-phase model then overestimates the gas density by $\approx \sqrt{1.5} = 1.22$. Given that the X-ray surface brightness is $\propto 1/R$ within the cooling radius, the contribution of the cooling component would be independent of radius in a steep potential, whereas the cooling gas would be more centrally concentrated in a flat potential (Thomas et al. 1987).

3. CONSTRAINING THE MASS DISTRIBUTION IN A1689

We use the X-ray surface brightness profile from the ROSAT PSPC (most closely related to the gas density), combined with the broad-band integrated temperature to constrain the normalization for a range of different-shaped mass profiles. We therefore derive a range of mass surface density profiles (under the assumptions of smooth spherical potentials, hydrostatic equilibrium, and thermal support), which we then compare to the positions of the larger lensed arclets and to the mass derived from the full lensing analysis.

3.1. *Mass constraints from X-ray observations*

We use three differently shaped mass distributions, each with several possible core radii, in addition to the standard β-model. Model A is a β-model with $\beta = 1$ (see equation 1), model B a "softened isothermal" potential with

$$\rho(r) = \frac{\rho_0}{(1+(r/r_0)^2)} \tag{3}$$

and model C, which is a generalization of model B, as used by Miralda-Escude & Babul (1995), which has

$$\rho(r) = \frac{\rho_0}{(r/r_0)^\alpha (1+(r/r_0))^{\gamma-\alpha}} \tag{4}$$

and $\gamma = 2$ and $\alpha = 1$. We note that for the parameters used, model C closely approximates the potential model used by Thomas et al. (1987) in their detailed modelling of the X-ray emission from the cooling region within the cluster core. In model A the radius at which the mass surface density is equal to half its central value is $1.05r_0$. The equivalent radius for model B is $1.73r_0$. For each mass model, the gas density and temperature are derived from the equation of hydrostatic equilibrium and the surface brightness profile by the deprojection technique of Fabian et al. (1981). Each mass model accurately describes a simulated 9 keV spectrum. For each mass model listed in Table 2, we show the temperature profiles, gas and total mass within r, and the mass surface densities in Figures 7, 8, and 9. An outer pressure boundary condition is required to uniquely specify the temperature solution, and we use a pressure corresponding to $P_0(8.53') = 1.0 \times 10^{-4}\,\mathrm{cm^{-3}\,K}$ for $H_0 = 50\,\mathrm{km\,s^{-1}\,Mpc^{-1}}$, $q_0 = 0$. We verify that, although changing the outer pressure by a factor of two changes the temperature solution at large radius by a similar factor, this has little effect on the temperature solution near the core and only a small effect $\lesssim 1$ keV on the broad band temperature. The mass profiles of Figure 8 should be considered not as true X-ray determinations of mass as a function of radius (as is possible with spatially resolved spectroscopy), but as indicators of the range of physically plausible mass profiles (with different core shapes and slopes at large radii $\rho(r) \propto r^{-2}$ to r^{-3}) that are consistent with the current X-ray data. As the assumed shape of the potential is changed, the broad-band temperature most closely constrains the mass within a radius $\approx 1.5'$ which contains half the cluster X-ray emission (Figure 8). The more centrally concentrated potentials shown are not directly ruled out by these data, but would require the temperature profile of A1689 to be very different from those of better observed, nearby clusters. A key conclusion from Figure 8 is that although these representative mass distributions display a wide variety of temperature profiles (Figures 7), the resulting total masses vary by no more than a factor of two from 0.2 – 2.0 Mpc.

The mass surface density for a given temperature profile will be increased, if the cluster is elliptical and extended along the line of sight. We quantify this factor by modelling the cluster as a prolate spheroid. The gravitating mass density is assumed constant on similar ellipsoids, with density as a function of radius along the minor axis given by one of the spherical models above. The gas temperature and density are then assumed constant on the derived set of equipotentials, and found from the observed surface brightness profile by deprojection. The largest observed ellipticities of X-ray isophotes (and hence cluster potentials) are ≈ 0.2, implying an axis ratio of $\lesssim 1.75$ for the gravitating mass distribution (Buote & Canizares 1992). The projected surface mass density for a given temperature is then increased by the factor ≈ 1.3.

3.2. *Comparison of X-ray and Lensing Cluster Masses*

A1689 shows many small, tangentially elongated arclets, and several larger, fainter arcs (Soucail et al. 1988; Lynds & Petrosian 1989, Tyson and Fischer 1995). The positions of the larger arcs are sketched in Figure 2. The parameters of those nearest to the cluster center at a radius of $\approx 45''$ are given in Table 3. There are also two arcs at larger radii $\approx 75''$ to the NE which are near relatively bright galaxies.

We may make a simple comparison to the lensing properties of the potentials consistent with the X-ray data, which are close to circular in the plane of the sky. A circularly symmetric lens will magnify an on-axis background source into a ring shaped image, seen at a radius r such that the mean mass surface density $\bar{\Sigma}(<r)$ within r is equal to the distance-dependent critical density,

$$\bar{\Sigma}(<r) = \Sigma_{\rm crit} \equiv \frac{c^2}{4\pi G}\left(\frac{D_{\rm d}D_{\rm ds}}{D_{\rm s}}\right)^{-1} \tag{5}$$

where $D_{\rm d}$, $D_{\rm s}$, and $D_{\rm ds}$ are respectively the angular diameter distances from the observer to lens, observer to source, and lens to source. The radial magnification depends on the distribution of the lensing mass with radius, and the observed thinness of the arcs then provides a qualitative diagnostic for the central concentration (Hammer 1991). In terms of $\bar{\Sigma}(<r)$ and the actual surface density, $\Sigma(r)$, at r, the radial magnification is

$$m_{\rm r}(r) = 0.5\left(1 - \frac{\Sigma(r)}{\bar{\Sigma}(<r)}\right)^{-1} \equiv -\left(\frac{d\ln(\bar{\Sigma}(<r))}{d\ln r}\right)^{-1} \tag{6}$$

A point mass, a singular isothermal sphere, and a plane sheet give radial magnifications $m_r(r) = 0.5, 1$ and infinity, respectively. Small off-axis source displacements produce two large arcs, while larger displacements produce smaller arcs. The observations of single arcs in clusters rule out such symmetric lenses. However, more realistic potentials with roughly isothermal shapes, core radii lying within the arc radius, and moderate ellipticity have been shown capable of reproducing, in detail, the arcs observed in well studied clusters (see Mellier et al. 1996 for a recent review).

In Figure 9 we compare the mass models consistent with the X-ray observations of A1689, with the critical density at the distance of A1689 for plausible background source redshifts in the range $0.7 < z_s < 2$. Taking mass model C as a representative example and a source redshift $z_s = 1$, the smoothly distributed spherical component consistent with the X-ray measurements and a 9 keV temperature provides only 0.50 of the critical density at the arc radius of 45″. An axis ratio for the dark matter of 1.75:1 aligned along the line-of-sight increases this to 0.66, while this ellipticity combined with an X-ray temperature of 12 keV increases the fraction to 0.87. Based on an analysis of arclets in A1689, Tyson and Fischer (1995) determined the projected mass within the critical radius of 200 kpc to be $3.6 \times 10^{14}\,M_\odot$ with a power law dependence of $n = -1.4$ for the projected surface mass density out to a radius of 2 Mpc. At all radii, the mass inferred from lensing significantly exceeds that derived from the X-ray analysis. For example, the lensing analysis yields masses of $4.0 \times 10^{15}\,M_\odot$ and $5.4 \times 10^{15}\,M_\odot$ within radii of 2 and 3 Mpc respectively. The isothermal β model for the X-ray mass yields corresponding masses of $1.6 \times 10^{15}\,M_\odot$ and $2.4 \times 10^{15}\,M_\odot$. The X-ray measured masses are more than two times smaller than those inferred from the lensing (see also Figure 8). In the next sections we discuss the uncertainties in the X-ray mass determination and then discuss the evidence for the presence of mass substructure along the line of sight which could significantly reduce the discrepancy between the two mass measurements.

3.3. *Uncertainties in the X-ray Mass Determinations*

The two principle concerns with the accuracy of the X-ray mass determinations are associated with violations of the underlying assumptions. First, there is the possibility that nonthermal pressure support, notably from magnetic fields, could be important. Second, the hydrostatic assumption could be violated, if there are significant bulk flows present in the gas. We address each of these questions in turn and show that, while they can provide some uncertainty in the measured values, it is not likely that either effect can account for the large discrepancy observed in A1689.

Magnetic fields are likely to exist in the intracluster gas, but present limits suggest that their magnitudes are too small to affect the pressure balance. A survey of cluster rotation measures showed that, generally, magnetic fields are of order 1 microgauss (Kim, Kronberg & Tribble 1991). The exceptions are within cluster cores around the bright central galaxies, but these magnetic fields are too localized to supplement the thermal pressure over a large volume. Thus, the observed magnetic fields throughout the intracluster gas are too small to invalidate the assumption of thermal pressure support.

A second argument that the gas is supported by its own thermal pressure is that the gas temperature is appropriate to the gravitational potential in which it lies. Generally, the energy per unit mass in galaxies, β_{spec}, is comparable to or less than that in gas. Specifically, $\beta_{spec} = \mu m_H v^2 / 3kT_{gas} \sim 1$ where v is the cluster velocity dispersion and T_{gas} is the gas temperature. This implies that for the gas, there are no unaccounted for pressure terms. In fact, as discussed in section 4, for clusters without apparent substructure, the average $\beta_{spec} < 1$, which means that the gas is somewhat hotter than the galaxies, which is readily explained as arising from the energy injected into the intracluster medium when the intracluster gas was enriched with iron during an early galactic wind from the galaxies.

Now, we address the question of bulk flows. If there are large bulk flows, then the assumption of hydrostatic equilibrium is invalid. The magnitude of this effect is best addressed through numerical experiments which can model the observational analysis procedure for simulated clusters. One of the most detailed studies of the validity of the X-ray cluster mass determinations was carried out by Evrard, Metzler & Navarro (1996) who concluded that the simplest X-ray analysis – an isothermal β-model (Cavaliere & Fusco-Femiano 1976) – is remarkably robust. In this model, the X-ray surface brightness is characterized by equation 1) and the temperature profile is assumed to be isothermal. These assumptions, with the hydrostatic equation, yield the following expression for the mass interior to the radius R:

$$M(<R) = \frac{3\beta k}{G\mu m_p} \frac{x^2}{(1+x^2)} T_{gas} R \qquad (7)$$

where $x = R/r_0$ and μm_p is the mean molecular weight of the gas. For typical numerical values we have:

$$M(<R) = 1.02 \times 10^{15} \beta (x^2/(1+x^2)) \frac{T_{gas}}{(9keV)} \frac{R}{1Mpc}\,M_\odot \qquad (8)$$

For a set of 58 independent simulations, Evrard et al. compared the X-ray analysis to the true values of the mass. They found that inside a radius R_{500} where the mean over density exceeded $500\rho_{crit}$ where $\rho_{crit} = 3H_0^2/8\pi G$, the gas is in hydrostatic equilibrium to an accuracy of about 10% on average. In the simulations the expression for the ratio of the mass derived above to the true mass has a full range of about 50% about the mean, with a few outliers. In addition, the X-ray mass estimate at radii R_{500} is an *underestimate* for many models.

Evrard et al. suggest an alternate mass estimator with an even smaller dispersion. Based on their simulations, they find that the mass inside R_{500} can be accurately described as

$$M(<R_{500}) = 2.22 \times 10^{15} (T_{gas}/10\mathrm{keV})^{3/2}\,M_\odot \qquad (9)$$

This estimator of the mass has less dispersion than the standard isothermal β-model. Its maximum deviations are less than 40% for the variety of models that Evrard et al. explored.

With this estimator, we compute an upper bound to $M(<R_{500})$ for comparison to that calculated from the isothermal β-model and from gravitational lensing that is 40% higher than the value given by equation 9), or $2.7 \times 10^{15}\,M_\odot$. This upper bound is still 1.7 times smaller than the mass derived from the arclet analysis. The mass derived from the isothermal β-model, $M = 1.84 \times 10^{15}\,M_\odot$ (for $R_{500} = 2.35Mpc$), is nearly identical to the Evrard et al. best estimate. We also note that in the sample of simulations, clusters with significant substructure are not omitted from the analysis and that the "standard" analysis of bimodal or complex clusters results in mass estimates that are significantly different from the true mass. In conclusion, if A1689 is an extreme example of a cluster undergoing a high

velocity merger, then simulations show that the effects of bulk flows could contribute to underestimates of the total mass by up to 40%. However, the good agreement of the mass determined from the β model and that from the Evrard et al. temperature only method suggests that A1689 is not an extreme example of an ongoing merger, so the effects of bulk flows would be even less. Thus we cannot reconcile the lensing-derived masses with those from the X-rays based only on uncertainties in the X-ray measurements or violations in the underlying assumptions.

4. GALAXY RADIAL VELOCITIES AND SUBSTRUCTURE

Teague, Carter & Gray (1990; hereafter TCG) obtained radial velocities of 66 cluster members, estimating a cluster velocity of $55017 \pm 288\,\mathrm{km\,s^{-1}}$ and velocity dispersion $\sigma = 2355^{+238}_{-183}\,\mathrm{km\,s^{-1}}$ (without correcting to the cluster rest frame: their Table 8). However, they found that the velocity distribution was not well fitted by a normal distribution. They also noted that of the three bright galaxies within 20″ of the apparent cluster center, one (the brightest, galaxy 2 in the notation of TCG and Figure 2) is approximately at rest relative to the cluster with a radial velocity of $54816\,\mathrm{km\,s^{-1}}$, another (TCG3) has a radial velocity $+4767\,\mathrm{km\,s^{-1}}$ relative to this, and the third (TCG1) has a velocity of $-2686\,\mathrm{km\,s^{-1}}$ (this galaxy is classified as a dumbbell cD, with a relative velocity between the two components of $800\,\mathrm{km\,s^{-1}}$; Valentijn & Casertano 1988). Teague et al. (1990) also suggested that the decreasing velocity dispersion with increasing radius observed in A1689 resulted from the presence of a high velocity group superposed on the cluster core. With the exclusion of this group, the velocity dispersion was constant with radius for A1689, as was found for the other nine clusters in their survey sample.

An isotropic galaxy velocity distribution with a fraction β_{spec} of the thermal energy per unit mass of the X-ray gas will have a line-of-sight velocity dispersion of $1205\beta_{\mathrm{spec}}^{1/2}(kT/9\,\mathrm{keV})^{1/2}\,\mathrm{km\,s^{-1}}$. Assuming hydrostatic equilibrium for the gas and an isotropic distribution of galaxy velocities, a galaxy population distributed radially like the X-ray gas with $\rho_{\mathrm{gal}} \propto r^{-2}$ should have $\beta_{\mathrm{spec}} \approx 1$, and a population with $\rho_{\mathrm{gal}} \propto r^{-3}$ would have β_{spec} equal to 0.79, (the value from the fit to the X-ray surface brightness profile in Section 2.1). The average β_{spec} for a sample of 20 nearby clusters with little or no substructure in their X-ray images is 0.85 (Jones and Forman 1996), consistent with simple hydrostatic models for the gas. For 24 nearby clusters with substructure, the average β_{spec} is 1.30 with the largest value being 2.8. The higher values are likely due to the effects of superposition and substructure on the measured galaxy velocity distribution. The high velocity dispersion measured in A1689 corresponds to $\beta_{spec} = 3.9$ which is substantially larger than that measured for any nearby cluster. The uniqueness of A1689 considered as a single system is shown graphically in Figure 10.

We examined the distribution of measured galaxy velocities in A1689 and quantified deviations from a single normal distribution with a maximum-likelihood fit of a superposition of normal distributions to the unbinned velocities. Most of the discrepancy with a single-component normal distribution is contributed by the tail of galaxies with velocities $58000\,\mathrm{km\,s^{-1}} \lesssim v_{\mathrm{rad}} \lesssim 62000\,\mathrm{km\,s^{-1}}$. Adding a second gaussian component to the model gives a statistically significant decrease of 11 in the likelihood statistic (Δ C-stat, distributed like χ^2). The two components (solid lines in Figure 11) are centered at $54460 \pm 270\,\mathrm{km\,s^{-1}}$ with velocity dispersion in the cluster rest frame $\sigma = 1470^{+210}_{-160}\,\mathrm{km\,s^{-1}}$, and $59810 \pm 310\,\mathrm{km\,s^{-1}}$ with $\sigma = 650^{+250}_{-160}\,\mathrm{km\,s^{-1}}$ (errors are Δ C-stat = 1 corresponding to 67% confidence limits on a single interesting parameter).

The velocity dispersion of the dominant component is still too large to be consistent with the gas temperature, if the temperature reflects the cluster potential. Adding a third component (shown dotted) to the velocity model results in two subgroups with centers $55340 \pm 360\,\mathrm{km\,s^{-1}}$ and $52520^{+730}_{-390}\,\mathrm{km\,s^{-1}}$ and dispersions $860^{+270}_{-170}\,\mathrm{km\,s^{-1}}$ and $700^{+250}_{-190}\,\mathrm{km\,s^{-1}}$ but reduces the fit statistic only by 4, which is not a statistically significant reduction. However, there is other evidence for the plausibility of this decomposition into subcomponents. In particular, the central velocities of the three components coincide with the velocities of TCG2 (the brightest cluster galaxy), TCG1 (the dumbbell cD and therefore likely to be near the dynamical center of a subcluster), and with TCG3. With three components, the velocity dispersion of the velocity component centered on TCG2 (at the X-ray centroid) is consistent with the X-ray temperature. β_{spec} values for the dominant cluster in both the two and three component decompositions are shown in Figure 10.

Thus for A1689, we conclude that there may be at least two and possibly three subclusters superimposed along the line of sight. The suggestion of superposition is consistent with the unusually high galaxy richness of A1689 (Abell richness class 4). If we make the assumption that mass follows light and assign galaxies with measured velocities to subclumps, we may estimate the contribution of the superimposed subcluster centered on TCG3 to the projected mass. Of the 68 galaxies with radial velocities measured by TCG, within 0.25° and $\pm 7000\,\mathrm{km\,s^{-1}}$ of the brightest cluster galaxy, 9 are likely to be part of the subcluster at $+5000\,\mathrm{km\,s^{-1}}$. This implies that the TCG3 galaxy concentration has a mass which is 15–25% of the main A1689 concentration. Most galaxies in this subcluster are spatially associated with two faint arcs which lie 75″ to the NE of the center of A1689 (this could be the core of the subcluster).

The presence of substructure in A1689 is supported by the weak lensing analysis of Tyson and Fischer (1995) and the analysis of the radial magnification bias by Broadhurst (1995) in A1689. Tyson and Fischer already noted that the velocity dispersion of 2300 km $\mathrm{sec^{-1}}$, derived assuming the optical galaxies reflect a single relaxed system, was inconsistent with their weak lensing analysis. In addition, Broadhurst (1995) showed that a simple isothermal model with the mass characterized by the velocity dispersion, $\sigma = 2000\mathrm{km\,sec^{-1}}$ was clearly too large to account for the observed radial magnification bias. Hence, a comparison of the lensing data and the optical data show that the galaxy velocity data cannot arise from a single relaxed system.

Further support for the presence of substructure and superpositions comes from the numerical simulations of Bartelmann and Steinmetz (1996). They found that, of their 378 simulated clusters, all those with X-ray and lensing mass discrepancies comparable to those of A1689 showed multiple velocity peaks resulting from superpositions along the line of sight.

In the following, we discuss how the presence of substructure can resolve the apparent inconsistency between the cluster mass estimated from studies of arcs and from X-ray observations.

5. DISCUSSION AND CONCLUSIONS

Our ROSAT PSPC observations show that A1689 is nearly spherical in X-rays, is centered on the bright galaxy TCG2 at

the center of the lensing pattern, and, in X-rays, is structure free down to scales of 15″. We have used the X-ray data from ROSAT, Ginga, and ASCA to derive constraints on the cluster mass distribution for a wide range of assumed potential shapes. We assumed hydrostatic equilibrium to derive the radial temperature profile from the surface brightness profile and then normalized the integrated broad-band temperature to the measured ASCA value of 9 keV. The goal of our analysis was to determine the allowed range in gravitating mass determined from the standard X-ray analysis techniques (Bahcall & Sarazin 1977; Mathews 1978). By comparing the X-ray determined mass with new results from gravitational lensing mass determinations, we can test the assumptions underlying the various methods.

We find that the integrated broad-band X-ray temperature places strong constraints on the mass enclosed within the large arcs at radius 45″ (185 kpc). For various mass models, we find that the X-ray data constrain the mean surface density within 45″ to be between 44% and 54% of the critical density for an assumed source redshift $z = 0.7$ and a single, spherically symmetric cluster. The result is nearly independent of the model for the radial mass distribution, as the arcs enclose about 40% of the X-ray emission. A simple, smooth spherical potential can therefore provide only about 50% of the critical density within the large arcs, in agreement with the earlier results of Miralda-Escude & Babul (1995) from the Einstein data, and extending their analysis of this object by obtaining a constraint independent of the gas temperature profile or equivalently independent of assumptions about the core radius of the potential.

The mass of the cluster also could be higher, if the temperature of the primary cluster exceeds 9 keV, as derived from the simple fit to the ASCA and Ginga spectral data. For a spherical cluster mass model, a 12 keV temperature implies a mass density which is 67% of the critical density.

The largest ellipticities seen in X-ray clusters correspond to dark matter axis ratios of 1.75:1 (Buote and Canizares 1992). If A1689 were similarly prolate along the line-of-sight, this would increase the 'smooth' mass contribution by a factor 1.33 to 67% of the critical density. Ellipticity alone cannot then account for all of the discrepancy.

Since a single cluster apparently cannot provide a mass distribution consistent with both the gravitational lensing together with the conventional assumptions using the X-ray data, and since the galaxy velocity data and the presence of a dumbbell cD suggest the presence of substructure, we then examine the effects of subclustering. First, both the arc and galaxy velocity data show a subcluster $\approx 75''$ to the NE of the X-ray centroid (see Figure 11) which contains $\sim 15-25\%$ of the mass of the primary A1689 mass concentration. Since the X-ray luminosity scales as $L_x \propto M^{2.5}$, this subcluster will have only 1 - 3% of the X-ray luminosity of the main cluster and be "invisible" in X-rays. Two arcs at 75″ from the brightest cluster galaxy are near galaxies assigned to this subcluster (perhaps this is the subcluster core). However, based on the estimated mass of the subcluster relative to the main component, this subcluster could increase the mass projected within the radius of 45″ only to 58% of the critical density, even if the subcluster were exactly aligned.

A third mass concentration may exist around galaxy TCG1, a dumbbell cD, whose velocity differs by 2700 $\mathrm{km\,s^{-1}}$ from the velocity of the central bright galaxy TCG2 and 2320 $\mathrm{km\,s^{-1}}$ from the cluster mean. Such a large velocity difference for such a luminous (massive) galaxy suggests it lies at the center of its own mass concentration (Quintana & Lawrie 1982; Beers and Geller 1983; Kriss, Canizares & Cioffi 1983).

Thus, there may be at least two and possibly three mass concentrations tightly aligned along the line of sight around the center of the main A1689 cluster. Large scale structure is observed to be filamentary, and hence, the identification of one accurately aligned subcluster in A1689 (whose velocity coincides with TCG3) then increases the probability both that the cluster is prolate along the line-of-sight, and that additional mass concentrations are aligned along the line of sight. Note that the arrangement of three bright galaxies within 15″, yet widely separated in velocity at the center of A1689 is difficult to explain without recourse to superposition.

Consistency between the lensing and X-ray data, in the absence of substantial non-thermal pressure support for the gas, could be provided by the presence of aligned substructure in the core of the A1689 cluster. We identify two scenarios. The first is one in which there are three subclusters, as identified in Figure 11. All three of these subclusters would lie nearly along our line of sight. The second scenario is one in which the primary cluster is elongated along the line of sight, and either has the largest mass allowed by the present gas temperature constraints, or a contribution from the small superposed subcluster to which TCG3 belongs. An alignment of three subclusters, or one highly elliptical cluster and a subcluster is not unlikely in one extreme object such as A1689, given the fact that clusters are embedded in large scale sheets or filaments. Although the additional alignment with our line-of-sight would be fortuitous. As shown in Figure 9, the production of giant arcs at large radii, in general, requires more mass than is inferred from the typical cluster potential as characterized by the velocity dispersion and gas temperature. As simulations and detailed modelling of particular clusters have shown, large arcs at large radii can result from substructure or superpositions. Thus, selecting objects with such arcs may also select highly structured clusters in the process of merging.

In addition, to providing mass along the line of sight which may not be detected in the X-ray measurements, in certain cases, subclusters can affect the gravitational lensing mass determinations from the large arcs. For example Bartelmann (1995) showed that the enhanced tidal effects in asymmetric lenses (e.g., those arising from clusters with substructure) can produce erroneously high mass estimates. For a particular cosmological model ($\Omega = 1$, $H_0 = 50\,\mathrm{km\,s^{-1}\ Mpc^{-1}}$), Bartelmann (1995) found that mass determinations from long arcs, assuming they lie on the Einstein radius, are too large by a factor of 1.6, on average. This effect can contribute a significant portion of the mass differences between the X-ray derivations and lensing when assuming spherical symmetry for the formation of large lensed arcs. This bias does not affect the results of weak lens inversions. Thus while the X-ray cluster mass measurements are sensitive to the mass interior to the region where the gas has been shocked, the lensing analysis detects all the projected mass along the line of sight. In the presence of aligned subclusters, significantly more mass would be detected in projection. By comparing the lensing and X-ray determined masses, we can study the mass distributions on larger scales and can begin to disentangle the effects of projection. Thus, while we have argued that bulk flows or non-thermal support from magnetic fields are not sufficient alone to account for the large discrepancies in mass determinations for A1689, the superposition of substructure can account for the factors of two

(or more) difference in mass determinations and provide a consistent picture of the available observations. If ongoing mergers of subclusters are occurring, then bulk flows also will be present and could somewhat reduce the X-ray mass estimates from the standard β model.

Although there may be substructure and superposition in the field of A1689, the mass-to-light ratio of 200 ± 30 $M_\odot/L_\odot$ found by Tyson and Fischer agrees well with the values found by other recent studies. Notably, the CNOC group (Carlberg et al. 1996) find a mean mass-to-light ratio of 156 ± 15 $M_\odot/L_\odot$ (with sample variance of 55 $M_\odot/L_\odot$; corrected to the visual band) for 14 X-ray selected clusters, after excluding one deviant cluster. This is similar to the mass-to-light ratios of 100-150 $M_\odot/L_\odot$ found by David et al. (1995; see their Figure 2) for hot clusters at comparable radii from X-ray measurements. These recent determinations of the mass-to-light ratio are smaller than previous values e.g., Faber and Gallagher (1979) gave a median mass-to-light ratio of 290 $M_\odot/L_\odot$ for 15 clusters and Blumenthal et al. (1984) cited a value of 240 $M_\odot/L_\odot$ (converted to the visual band).

As a final question, we can ask whether giant lensed arcs *ever* reflect the surface density of a single, smooth, near-spherical potential. If we assume that the range of "reasonable" potentials we derive from the X-ray observations for A1689 are characteristic of other lensing clusters, we can then compare these to the radii at which giant arcs are observed in other clusters. In Figure 9, we have compared the scaled arc radii and critical densities for three clusters to our potential models for A1689. Note that the gas temperatures of these clusters lie in the range from 5 to 7 keV (Rines et al 1996), lower than that of A1689. Thus the estimated masses for these clusters from their X-ray measurements would be lower than the mass density shown for A1689. For A963 and MS2137-23, the arcs lie at small radii, and are consistent with the steeper potentials allowed for A1689, even if the masses are reduced to take the lower cluster temperatures into account. Allen et al. (1996) also found agreement between the mass derived from X-rays and that inferred from the giant arc in the cluster associated with PKS0745. As Allen et al. argued, the agreement in X-ray and lensing mass determinations does not require non-thermal gas pressure and demonstrates that the gas is in hydrostatic equilibrium. These systems are consistent with single, relaxed clusters. However, (like the arcs in A1689), the large arcs in A370 fall at radii which are too large to be due to a single cluster potential and in that case reflect substructure (this is revealed in the ROSAT HRI observation of A370 and is consistent with the detailed modelling of Kneib et al. 1993 which requires a bimodal potential to reproduce all the lensing properties). In general, cluster gas temperatures rarely exceed 9 keV, and only A2163 has been found to exceed 12 keV, so that the mass densities in Figure 9 are the largest expected. Thus the higher masses required by the presense of giant arcs at large radial distances require complicated lensing geometries (i.e., subclustering or superpositions).

Single mass concentrations, sufficiently compact to produce lensed giant arcs at small radii, will always imply gas densities high enough to initiate a cooling flow (note that this means that the gas density in the core is then no longer simply related to that predicted by simple dissipationless models of cluster formation). If the converse is also true, and cooling flows conceal potentials with cores steeper than a constant density isothermal sphere, then many of the EMSS survey clusters which are biased toward peaked X-ray surface brightness distributions (Pesce et al. 1990) would be capable of producing giant arcs, at least with critical radii $\lesssim 15''$ for $z_s = 2$. In fact, 30% of EMSS clusters show lensed arcs (Le Fevre et al. 1994).

Further information on the mass distribution, substructure, and physical state of the ICM in cluster cores will come from future comparisons of lensing and X-ray data. Such comparisons will require samples which are chosen to minimize potential biases such as those which would arise if clusters with coaligned substructure were systematically selected. Constraints on multiphase components will come from detailed X-ray spectroscopy and comparison of continuum and line temperatures. Comparison of radio Sunyaev-Zel'dovich maps with X-ray data will provide further information on the state of the hot intracluster gas and numerical simulations will yield a clearer understanding of the effects of substructure and bulk velocities in the gas.

ACKNOWLEDGEMENTS

We acknowledge helpful discussions with the referee, J. Miralda-Escude, whose comments helped clarify the discussion. We thank M. Arnaud and J. Hughes for providing the archival Ginga data and for advice with the analysis. We acknowledge helpful discussions with R. Narayan, A. Loeb, D. Fox, and M. Bartelmann. SJD acknowledges support from a Predoctoral Fellowship funded by the Smithsonian Institution. Research support was provided by the Smithsonian Institution, ROSAT Grant NAG5-1881 and the AXAF Science Center NAS8-39073.

REFERENCES

Allen, S.W., Fabian, A.C., Johnstone, R.M., White, D.A., & Daines, S.J. 1993, MNRAS, 262, 901

Allen, S.W., Fabian, A.C., & Kneib, J. 1996, MNRAS, 279, 615

Arnaud, K.A. 1988, In: *Cooling Flows in Galaxies and Clusters*, p.31, ed Fabian, A.C., Kluwer Academic Publishers, Dordrecht.

Bahcall, J., & Sarazin, J. 1977, ApJ, 213, L99

Bartelmann, M. & Steinmetz, M. 1996, Astro-ph/9603101

Bartelmann, M. 1995, A&A, 229, 11

Beers, T., & Geller, M. 1983, 274, 491

Blumenthal, G., Faber, S., Primack, J. & Rees, M. 1984, Nature, 311, 517

Broadhurst, T. 1995, astro-ph/9511150

Buote, D.A.& Canizares, C.R. 1992, ApJ, 400, 385

Carlberg, R. G., Yee, H. K. C., Ellingson, E., Abraham, R., Gravel, P., Morris, S., & Pritchet, C. J. 1996, ApJ, 462, 32

Cavaliere, A., & Fusco-Femiano, R. 1976, A&A, 49, 137

David, L., Jones, C., & Forman, W. 1995, ApJ, 445, 578

Donahue, M., Stocke, J.T., & Gioia, I.M. 1992, ApJ, 385, 49

Edge, A.C., Stewart, G.C., Fabian, A.C., & Arnaud, K.A. 1990, MNRAS, 245, 559

Evrard, A., Metzler, C. & Navarro, J. 1996, ApJ, 469, 494

Faber, S. & Gallagher, J. 1979, ARA&A, 17, 135

Fabian, A.C., Hu, E.M., Cowie, L.L., & Grindlay, J. 1981, ApJ, 248, 47

Grossman, S.A., & Narayan, R. 1989, ApJ, 344, 637

Hammer, F. 1991, ApJ, 383, 66

Hasinger, G., Boese, G., Predehel, P., Turner, T.J., Yusaf, R., George, I.M., & Rohrbach, G. 1993, MPE/OGIP calibration memo CAL/ROS/93-015

Hayashida, K., Inoue, H., Koyama, K., Awaki, H., Takano, S., Tawara, Y., Rees Williams, O., Denby, M., Stewart, G.C., Turner, M.L., Makishima, K., & Ohashi, T. 1989, PASJ, 41, 373
Henry, J.P., Briel, U.G., & Nulsen, P.E.J. 1993, A&A, 271, 413
Hewett, P.C., Foltz, C.B., Chaffee, F.H., Francis, P.J., Weymann, R.J., Morris, S.L., Anderson, S.F., & Macalpine, G.M. 1991, AJ, 101, 1121
Jedrzejewski, R. 1987, MNRAS, 226, 747
Johnstone, R.M., Fabian, A.C., Edge, A.C. & Thomas, P.A., 1992, MNRAS, 255, 431
Jones, C. & Forman, W. in preparation
Kim, K. T., Kronberg, P. P. & Tribble, P. 1991, ApJ, 379, 80
Kneib, J.-P., Mellier, Y., Fort, B. & Mathez, G. 1993 A&A, 273, 367
Kriss, G., Cioffi, D. & Canizares, C. 1983, ApJ, 272, 439
Le Fevre, O., Hammer, F., Angonin, M. C., Gioia, I. M., Luppino, G. A. 1994, ApJ Lett., 422, L5
Loeb, A., & and Mao, S. 1994, ApJ, 435, L109
Lynds, R., & Petrosian, V. 1989, ApJ, 336, 1
Mathews, W. 1978, ApJ 219, 413
Mellier, Y., Van Warebeke, L., Bernardeau, F., & Fort, B. 1996, astroph/9609197
Miralda-Escude, J. & Babul, A. 1995, 449, 18
Mushotzky, R.F., & Szymkowiak, A.E. In: *Cooling Flows in Galaxies and Clusters*, p.53, ed Fabian, A.C., Kluwer Academic Publishers, Dordrecht.
Ohashi, T. 1994 in Maryland Astrophysics Conference on Dark Matter (eds. S. Holt and C. Bennett), 255
Pesce, J.E., Fabian, A.C., Edge, A.C. & Johnstone, R.M., 1990, MNRAS, 224, 58
Quintana, H. & Lawrie, D. 1982, AJ, 87, 1
Rines, K., Forman, W., Jones, C., Donnelly, H. 1996, BAAS.
Sarazin, C. 1988, *X-ray Emissions from Clusters of Galaxies*, C.U.P.
Smail, I. Ellis, R., Fitchett, M. 1994, MNRAS, 270, 245
Soucail, G., Mellier, Y., Fort, B., Mathez, G., & Cailloux, M. 1988, ApJ, 119, L19
Squires, G., Neumann, D., Kaiser, N., Arnaud, M., Babul, A., Bohringer, H., Fahlman, G., & Woods, D. 1996a, astro-ph/9603050
Squires, G., Kaiser, N., Fahlman, G., Babul, A. & Woods, D. 1996b, astro-ph/9602105
Stark, A. etal, 1992, ApJS, 79, 77
Teague, P.F., Carter, D., & Gray, P.M. 1990, ApJ Supp., 72, 715 (TCG)
Thomas, P.A., Fabian, A.C., & Nulsen, P.E.J. 1987, MNRAS, 228, 973
Tyson, J.A., Valdes, F., & Wenk, R.A. 1990, ApJ, 349, L1 (TVW)
Tyson, J.A., & Fischer, P. 1995, ApJ, 446, L55
Valentijn, E.A., & Casertano, S. 1988, A&A, 206, 27
White, D.A., Fabian, A.C., Johnstone, R.M., Mushotzky, R.F., & Arnaud, K.A. 1991, MNRAS, 252, 72

Table 1: Spectral Fits

Model	kT (keV)	$\dot{M}$ ($M_\odot\ yr^{-1}$)	Abundance (solar[a])	χ^2 / d.o.f.
ROSAT Spectral Fits[d]				
1T ($1' - 5'$ ann)	$10.7^{+11.1}_{-4.0}$	—	0.29	27.6 / 29
1T ($0' - 1'$ ann)	$3.9^{+1.0}_{-0.7}$	—	0.29	20.2 / 27
1T + CF ($0' - 1'$ ann)	9	514^{+183}_{-183}	0.29	21.7 / 27
1T + CF ($0' - 5'$ ann)	9	490^{+209}_{-209}	0.29	31.1 / 29
Ginga + ROSAT Joint Spectral Fits				
1T + CF	$8.1^{+0.8}_{-0.6}$	331^{+230}_{-240}	$0.32^{+0.08}_{-0.08}$	66 / 53
1T + CF + soft[b]	$9.0^{+0.9}_{-0.8}$	340^{+220}_{-130}	$0.38^{+0.10}_{-0.10}$	68 / 53
1T + CF[c]	$11.2^{+1.2}_{-0.9}$	450^{+200}_{-200}	$0.31^{+0.08}_{-0.08}$	77 / 53
1T + CF + soft[b,c]	$12.8^{+1.7}_{-1.1}$	398^{+170}_{-170}	$0.38^{+0.09}_{-0.08}$	81 / 53
ASCA Spectral Fits				
1T	$8.98^{+0.45}_{-0.41}$	—	$0.29^{+0.06}_{-0.07}$	1428 / 1403
ASCA + ROSAT Joint Spectral Fits				
1T	$8.81^{+0.42}_{-0.40}$	—	$0.30^{+0.06}_{-0.07}$	1466 / 1434 (ASCA 0.7-9.0 keV)
1T + CF	$10.1^{+1.6}_{-1.2}$	579^{+271}_{-295}	$0.33^{+0.10}_{-0.09}$	1308 / 1295 (ASCA 1.5-9.0 keV)

[a] Relative to $Fe/H = 4.68 \times 10^{-5}$

[b] "soft" indicates that a 3 keV component has been included in the fit with the appropriate normalization to account for the other clusters in the Ginga field of view

[c] For these spectra an alternate background subtraction was used based on the average of many fields (see text)

[d] Parameters with no errors indicate fixed values derived from other fits.

Table 2: Summary of Mass Models

Shape	r_0 arcmin	linestyle
"β-model"	1.1	thick dashed
A	0.81	solid
A	0.40	dashed
A	0.20	dash-dot
B	0.40	dotted
B	0.20	dash-triple-dot
C	0.40	thick solid

Table 3: Long Arcs

long Arcs (primary)	PA (deg)	Length (deg)	Radius (arcsec)
A	228	28	47
B	12	23	47
C	130	9	43
D	173	10	76

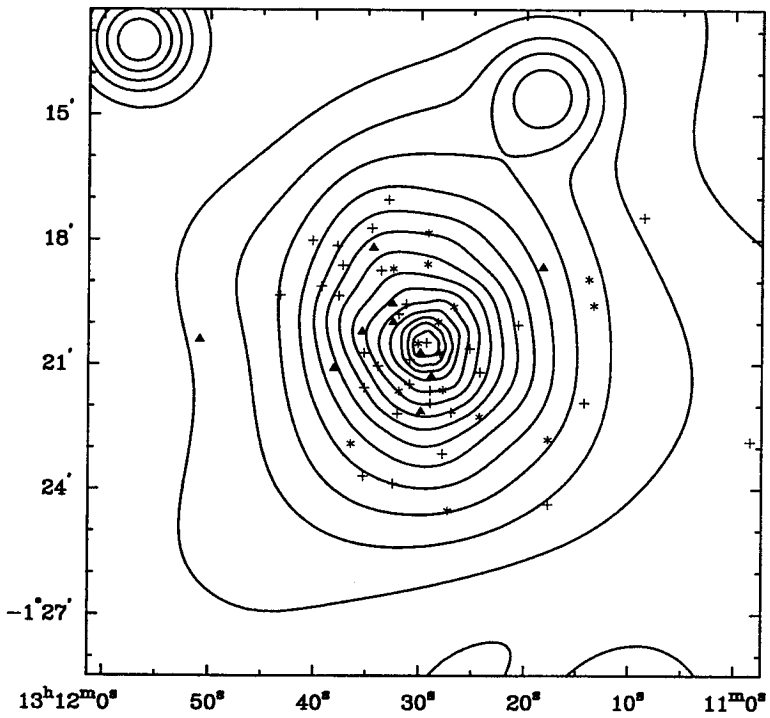

Fig. 1.— X-ray isointensity contours from ROSAT PSPC observation of A1689, in energy range 0.4 - 2.0 keV. The image was smoothed with an adaptive gaussian kernel, with smoothing scales from $\sigma = 6''$ to $\sigma = 160''$. Contour levels are at 6.31×10^{-4}, 1.0×10^{-3}, 1.58×10^{-3}, 2.51×10^{-3}, 3.98×10^{-3}, 6.31×10^{-3}, ..., 0.251 cts arcmin^{-2}s^{-1}. The background level is 3.71×10^{-4} cts arcmin^{-2}s^{-1}. Positions of galaxies with radial velocities measured by Teague et al. (1990) are overlaid, coded by velocity: $\triangle$ $5.8 \times 10^4\,\mathrm{km\,s^{-1}} < v_{\mathrm{rad}} < 6.3 \times 10^4\,\mathrm{km\,s^{-1}}$, $+$ $5.37 \times 10^4\,\mathrm{km\,s^{-1}} < v < 5.8 \times 10^4\,\mathrm{km\,s^{-1}}$, $*$ $4.75 \times 10^4\,\mathrm{km\,s^{-1}} < v < 5.37 \times 10^4\,\mathrm{km\,s^{-1}}$.

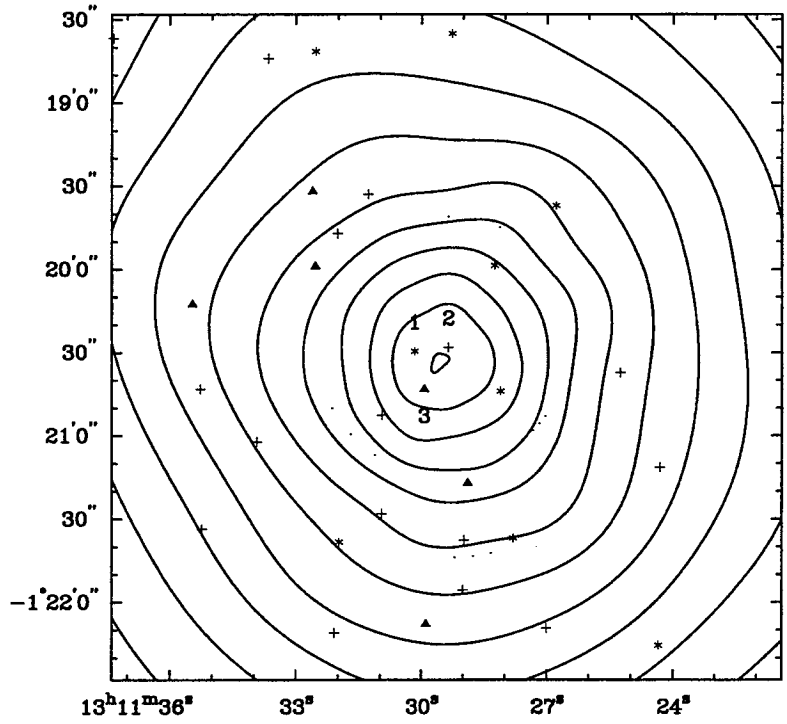

Fig. 2.— Inner part of Figure 1 on an expanded scale. Galaxies TCG1, TCG2, TCG3 are labelled and faint arcs from TVW are sketched.

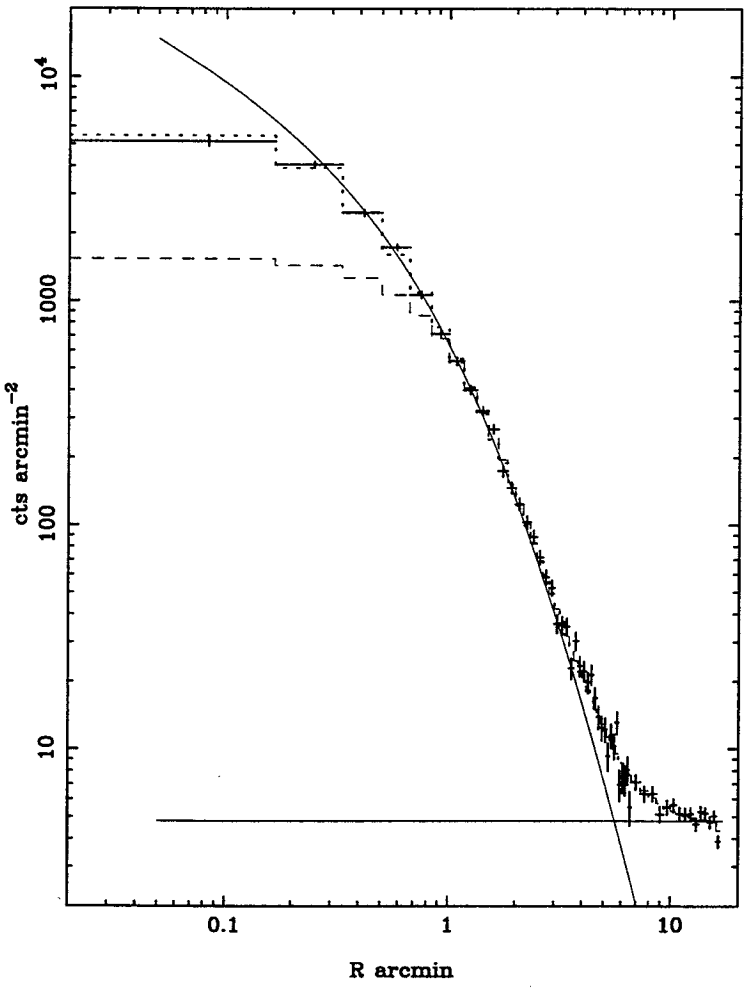

Fig. 3.— Model fits to the radial surface brightness profile with vignetting-corrected counts from the energy range 0.4 to 2.0 keV. The dashed line is a β-model fit excluding the inner 5 bins. The dotted line is a fit of the functional form of equation 2, also folded through the PSF. Thin solid lines are the unconvolved source and background components of this fit.

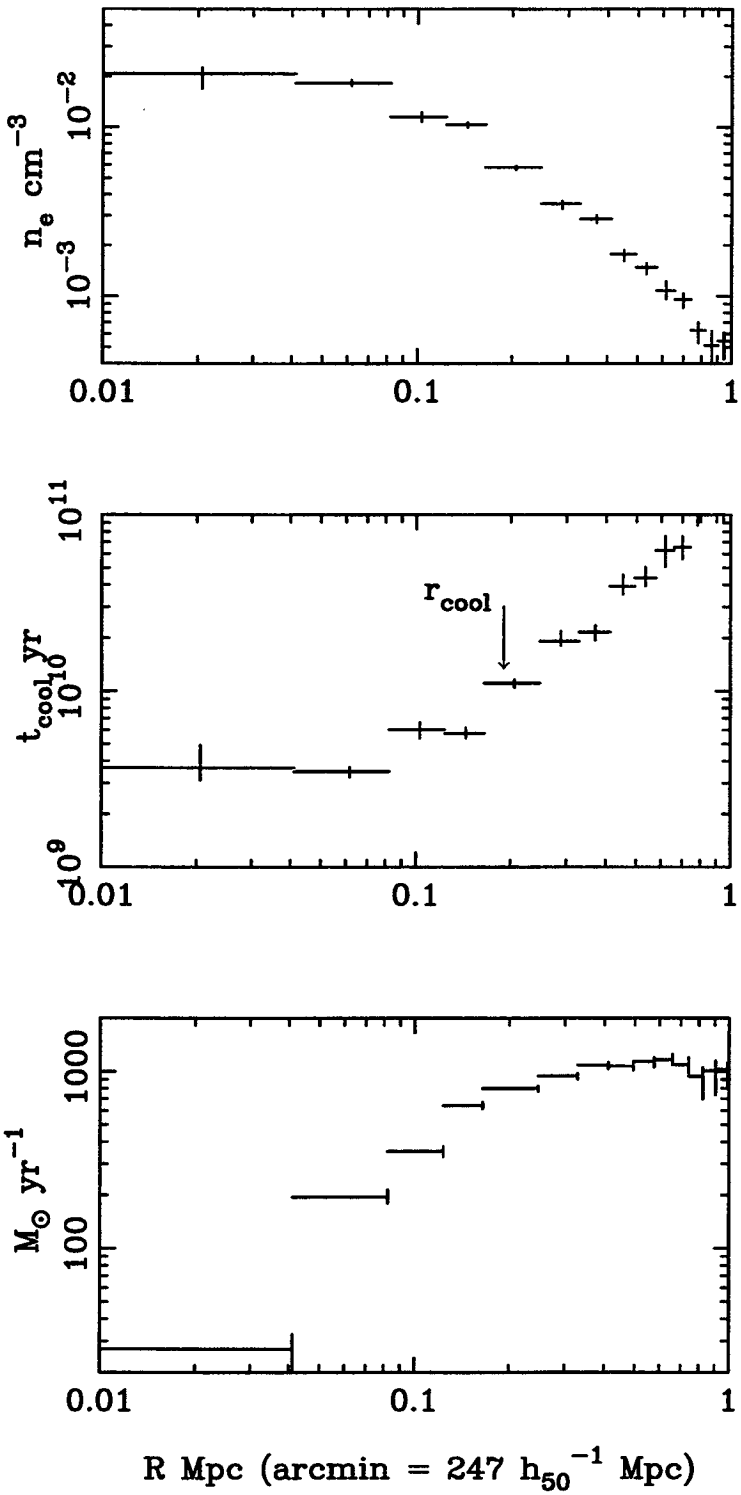

Fig. 4.— Results of single-phase deprojection analysis of the ROSAT PSPC surface brightness profile: (a) electron density, (b) cooling time, (c) mass deposition rate.

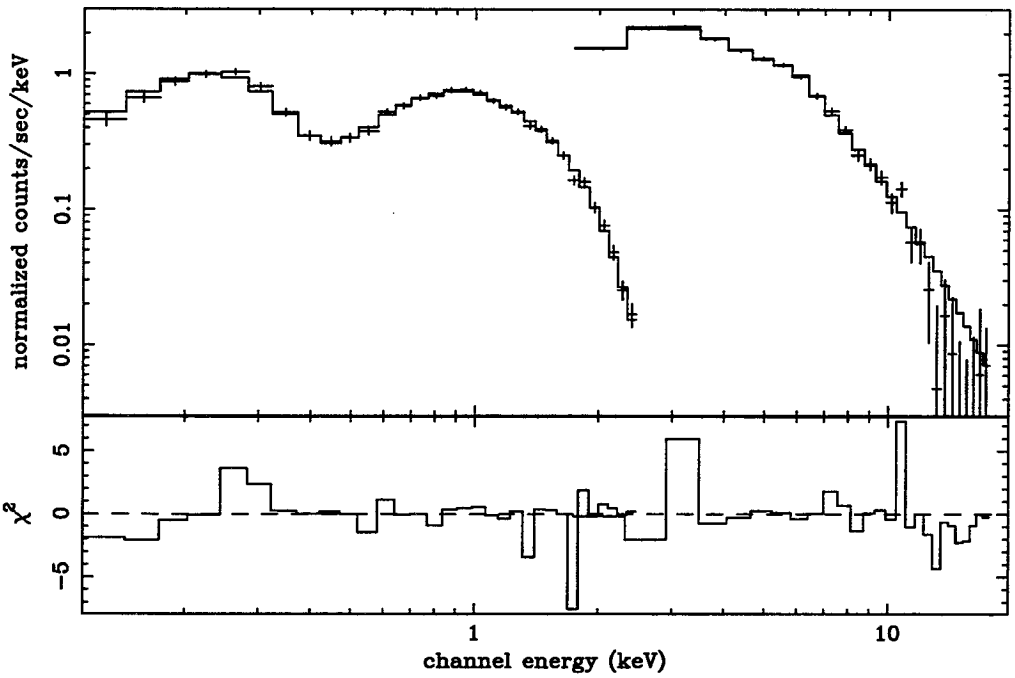

Fig. 5.— (a) ROSAT + Ginga spectrum of A1689, with best-fitting isothermal + cooling flow model (Ginga background is 'direct + soft' of Table 1). (b) Residuals from the fit. The structure in the energy range 0.2 - 0.4 keV is comparable to the difference between the two latest PSPC calibrations, and also to that seen due to temporal gain changes in the PSPC.

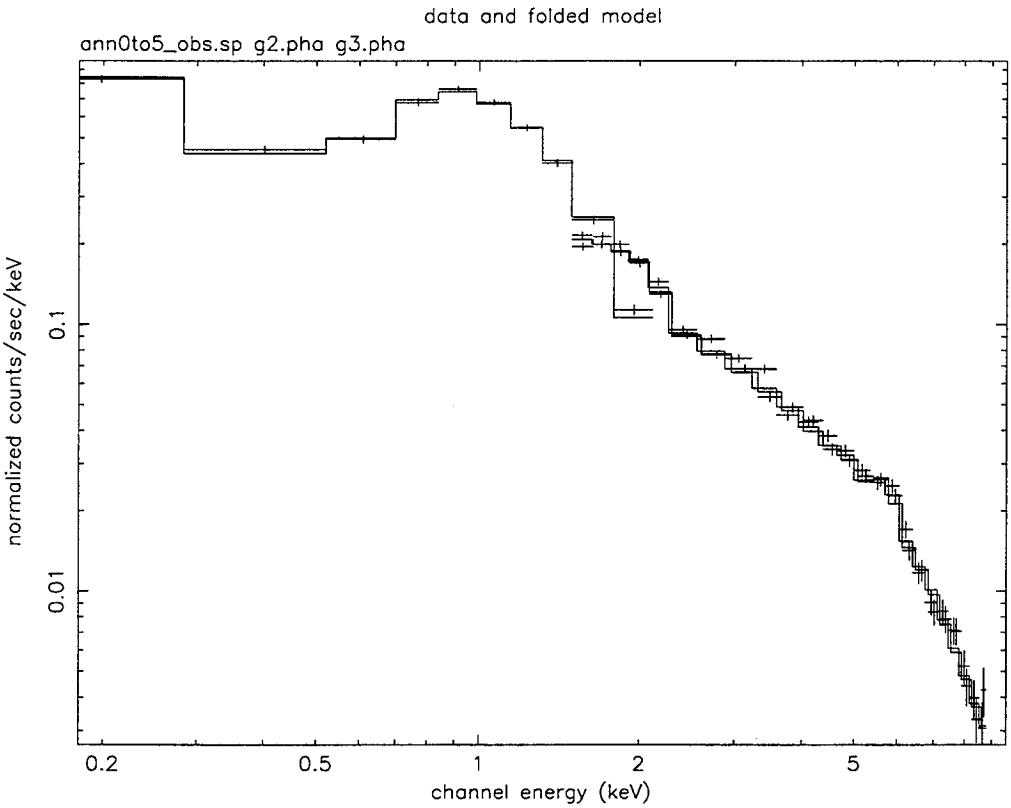

Fig. 6.— ROSAT + ASCA GIS spectrum of A1689, with best-fitting isothermal + cooling flow model. The data are binned for display only, to facilitate clarity in the plot. The resulting fit parameters given in Table 2 are fully consistent with the cooling flow measured in the spectrum of the central 0'-1' arc minute ROSAT annulus and in the deprojection analysis of the surface brightness.

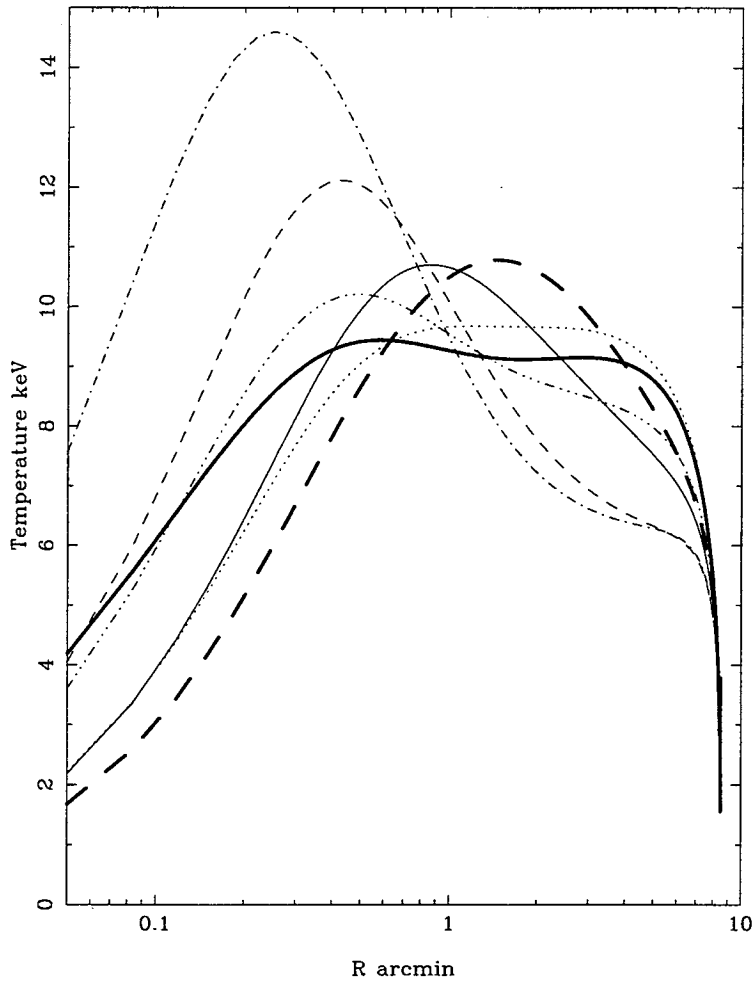

Fig. 7.— Radial temperature profiles for the potential models summarized in Table 2.

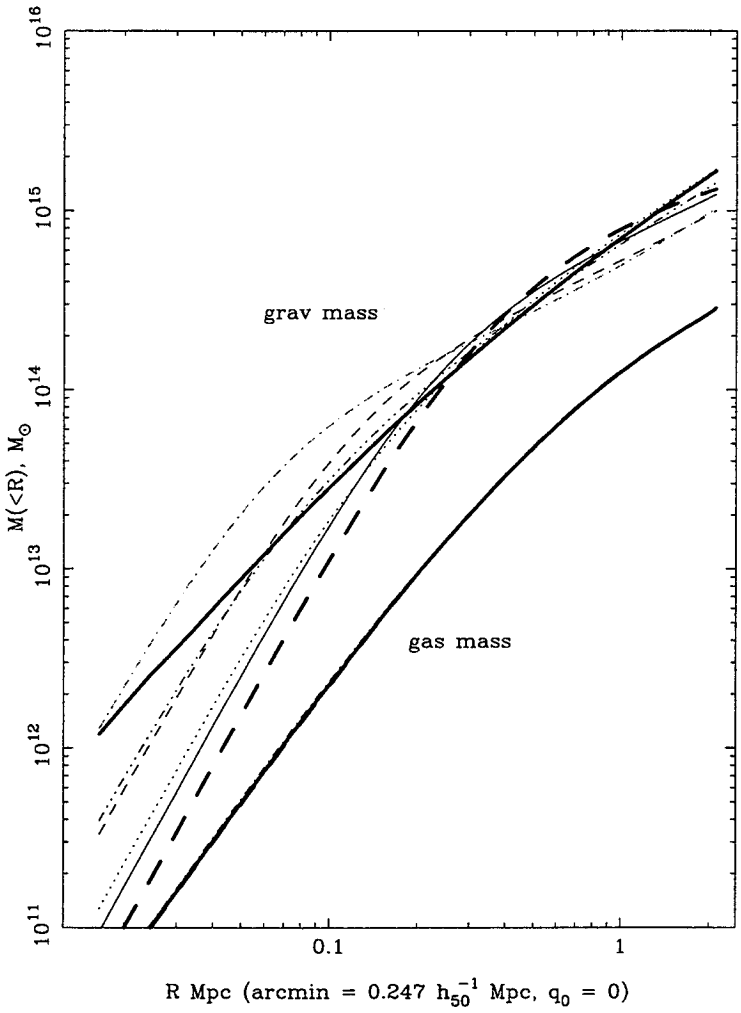

Fig. 8.— Total and gas mass for each model in Table 2 (lines for gas mass overlap) The total mass is best constrained by the integrated broad band temperature at radius $\approx 1.5'$, ($375h_{50}$ kpc) which encloses $\approx 50\%$ of the total counts. Under the standard assumptions of equilibrium and hydrostatic support, the X-ray derived projected masses are all below those determined directly via weak and strong lensing.

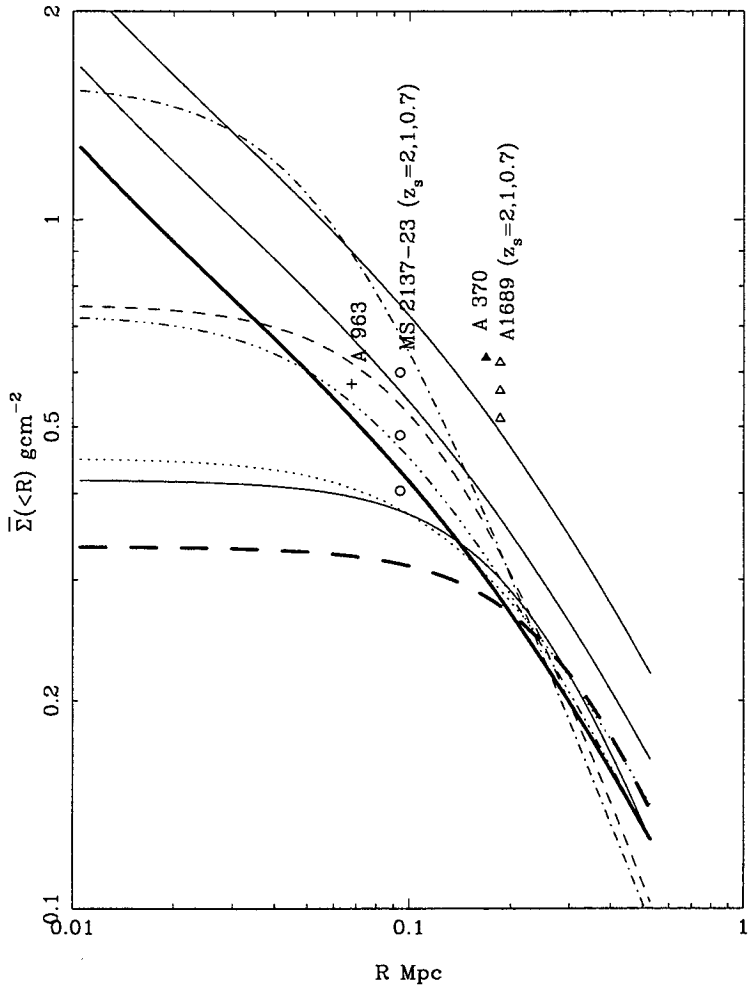

Fig. 9.— Mean surface mass density (within a cylinder at radius R) for each potential. The positions of large arcs in A1689 are shown. For comparison, arcs from several other clusters are overlaid on the A1689 mass models. Markers are plotted at the radii of large arcs from the center, and at the critical density for each cluster redshift and background source redshift (if known). Two additional thin solid lines show the surface density of model C (i) for a dark matter ellipticity of 1.75:1 (ii) for a dark matter ellipticity of 1.75:1 and higher broad beam temperature of 12 keV.

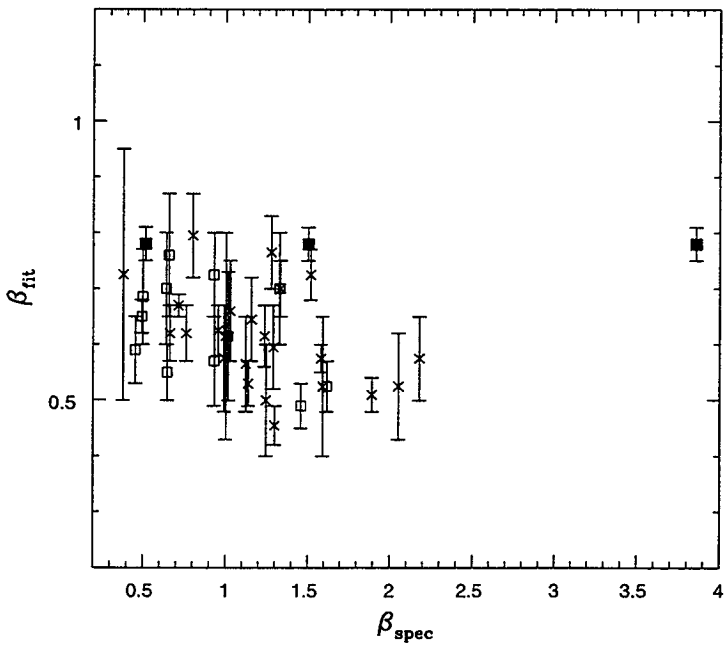

Fig. 10.— The values of β_{fit} derived from fitting X-ray surface brightness profiles are compared to β_{spec} computed from the measured velocity dispersions and gas temperatures for clusters with substructure (diagonal cross), without substructure (open square), and A1689 (filled squares). The three values for A1689 correspond to the three quoted in the text assuming 1, 2, and 3 Gaussian components.

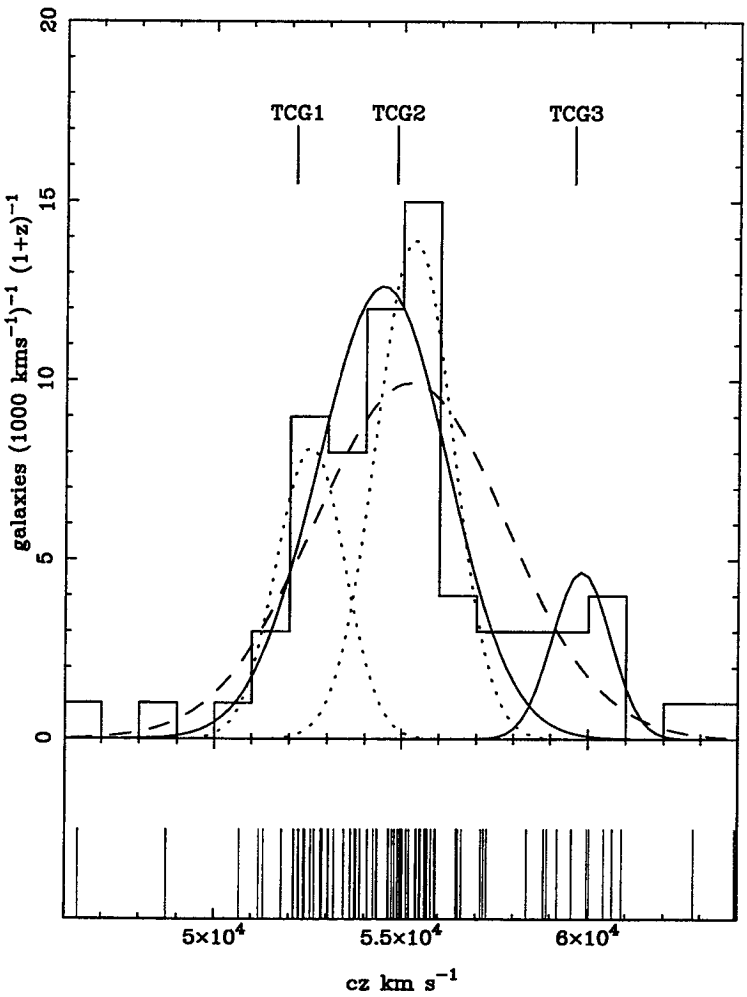

Fig. 11.— Galaxy radial velocities from TCG for galaxies within 0.25°of the brightest cluster galaxy TCG2. One, two and three component gaussian models are overlaid. These are described in Section 4.

DRAFT VERSION MARCH 7, 1997
Preprint typeset using LaTeX style emulateapj

ABELL 2218: X-RAY LENSING, MERGER, OR BOTH?

MAXIM MARKEVITCH[1]
Harvard-Smithsonian Center for Astrophysics, 60 Garden St., Cambridge, MA 02138; maxim@head-cfa.harvard.edu

Draft version March 7, 1997

ABSTRACT

Comparison of the high resolution X-ray image of A2218 obtained with *ROSAT* HRI with the optical *HST* image shows several interesting correlations. The X-ray emission within a $1'$ radius core is resolved into several components, with the central dominant galaxy not coinciding with either of them or the emission centroid. The major X-ray peak is an elongated feature which coincides with optical arcs at $r \simeq 20''$ from the cD and lies between the two mass concentrations known from the optical lensing analysis. We speculate that this may be lensed X-ray emission, for example (but not necessarily) of the same object lensed in the optical. Alternatively, this feature may be a merger shock, or a gas trail of an infalling subgroup, a possibility supported by the X-ray appearance on the larger angular scale. The *ROSAT* angular resolution is insufficient to distinguish between the lensing and merger possibilities, although both are likely. Two other X-ray enhancements are close to the two mass concentrations.

A2218 is a cluster with a lensing/X-ray mass discrepancy. Previous hydrostatic derivations of the A2218 mass used a β-model fit to the data with angular resolution that blurred the features mentioned above into a broad constant core. As the HRI data show, such a core doesn't exist. If, for example, a head-on merger is underway and assuming the cD has been at the center of the nearest X-ray peak in the past, then the hydrostatic estimate of the projected mass within the lensing radius can easily be increased by a factor of at least ~ 1.4 (and the mass within a sphere of the same radius by a factor of 2.6) compared to the β-model used in previous analyses. However, for a merging cluster, the hydrostatic analysis is generally inapplicable. Note that most other lensing clusters are more distant than A2218 and obtaining adequate X-ray images and temperature maps of those clusters is even more difficult. Together with the likely overestimation of mass by the lensing analysis (as in the simulations), oversimplification of the gas density and temperature models as a result of inadequate resolution may account for the lensing/X-ray mass discrepancy.

Subject headings: Dark matter — galaxies: clusters: individual (A2218) — intergalactic medium — lensing — X-rays: galaxies

1. INTRODUCTION

A2218 at $z = 0.175$ shows a strong discrepancy between cluster masses derived from gravitational lensing in the optical and from X-ray analysis (Miralda-Escudé & Babul 1995; Loeb & Mao 1994). In A2218 as well as in some other clusters (e.g., Wu & Fang 1997 and references therein), lensing implies a projected mass within the cylinder delineated by the observed giant arcs up to 2–3 times greater than the value derived from X-ray data assuming hydrostatic equilibrium, isothermality and spherical symmetry. Weak lensing results (e.g., Squires et al. 1996 and references therein) are consistent with strong lensing, although these results are still rather uncertain. Assuming that the mass from lensing is correct, Loeb & Mao (1994) proposed the existence of significant nonthermal gas support in the centers of clusters, due for example to gas turbulence or magnetic fields, which would compensate for the insufficiency of thermal pressure. Cluster simulations by Bartelmann (1995) showed that the spherically-symmetric lensing analysis should on average overestimate the true mass by a factor of 1.6 due to the presence of substructure. The remaining discrepancy is still significant and requires further explanation.

Makino (1996) proposed a declining temperature profile to account for the mass discrepancy in A2218; Loewenstein (1997) detected a temperature decline in the outer ($r >$ a few arcmin) region of the cluster but found it insufficient to explain the discrepancy. A2218 has one of the largest values of $\beta_T \equiv \mu m_p \sigma_{\rm gal}^2 / T_e \simeq 1.6$ (where $T_e = 7.2$ keV, Mushotzky & Loewenstein 1997, and $\sigma_{\rm gal} = 1370$ km s^{-1}, Le Borgne et al. 1992), which is a likely indication of the cluster's nonrelaxed state (e.g., Navarro et al. 1995). Kneib et al. (1995) and Squires et al. (1996) analyzed the *ROSAT* X-ray data on A2218 along with the lensing data, and noted that the X-ray image suggested an ongoing merger of subclusters. Below we discuss interesting details from a longer and better-positioned *ROSAT* HRI dataset, comparing it with the optical *HST* image from Kneib et al. (1996) to further investigate the nature of the mass discrepancy. Although strong temperature gradients in the inner region are likely if there is a merger, we will not consider their effects on the mass estimate and will limit the discussion to the imaging data only.

2. HRI IMAGE

The *ROSAT* HRI performed four observations of A2218, two of which (with a total exposure of 35.6 ks) are on-axis and two others offset by $12'$. We use only the on-axis pointings in which the HRI PSF at the position of interest has a half-power diameter of $4''$ (see *ROSAT* Handbook). This compares to a PSF of $20''$ for the offset pointings, which is insufficient to resolve the small scale structure discussed below. Images for the two pointings with $5''$ pixels are generated using the software of S. Snowden and then co-added. There is a bright X-ray source $12'$ off axis in the HRI field of view, coincident with the star SAO17151. A *ROSAT* PSPC spectrum of this source is soft

[1]Also Space Research Institute, Russian Academy of Sciences

which is typical of stars; thus the identification is firm. This object was used to correct for a $\sim 3''$ error in the *ROSAT* sky coordinates in both pointings (such an error is well within the nominal range). The resulting sky coordinates of the X-ray image are accurate to $\sim 1-2''$.

HRI surface brightness contours are overlaid on the optical image in Fig. 1. The image shows a complex multi-peaked X-ray structure in the inner $1'$–$2'$ of the cluster. Neither of the X-ray peaks coincides with the cD galaxy, whose J2000 coordinates from the Digitized Sky Survey image are $\alpha = 16^h35^m49^s.2, \delta = +66°12'45''$. Kneib et al. (who used one-third of this HRI exposure) and Squires et al. (using the same dataset) reported coincidence of the cD and the X-ray peak, but most probably, they have forced it by introducing an additional offset (the X-ray image in the latter paper appears inverted north-south with respect to the optical image, therefore this is likely).

A standard β-model fit to the X-ray surface brightness profile centered at the emission centroid yields $a_x = 58''$ and $\beta = 0.63$, in agreement with the *Einstein* IPC (Birkinshaw & Hughes 1994) and *ROSAT* PSPC values (Squires et al. 1996). However, comparing the central $100'' \times 100''$ part of the image binned in $20''$ pixels to the two-dimensional β-model by means of a χ^2 test shows that this model is unacceptable at the 99.99% confidence due to the structures seen in Fig. 1.

3. DISCUSSION

3.1. *X-Ray Lensing?*

The major X-ray peak to the south of the cD has a bow-like shape and lies at the position of the brightest optical arc. Using the *HST* data, Kneib et al. (1996) found four lensed images of the same distant ($z = 0.7$) object along the east-to-south quarter of the $21''$ radius circle centered on the cD. One of these lensed images is this brightest arc and three others are point-like (see Fig. 1). The elongated X-ray structure covers about the same region. It is quite possible that lensed X-ray flux from the same object (or maybe other background X-ray sources) contributes to the central X-ray structure. Presently, such an interpretation is of course one of the many possibilities since this X-ray peak is also coincident with a bright spiral galaxy and the group surrounding it. The *ROSAT* HRI resolution is insufficient to determine whether the X-ray emission in the center consists of point- or arc-like sources or is extended. *AXAF* instruments will be able to resolve any X-ray lensing here. If lensing of distant sources contributes any considerable X-ray flux near the cluster center, it could modify the derived gas density profile and hence the X-ray mass estimate. X-ray lensing has been observed with the HRI in another object (Chartas et al. 1995).

3.2. *Subcluster Merger*

Another likely explanation of the observed X-ray structure is a subcluster merger. From the lensing data, Kneib et al. (1995, 1996) detected two major mass concentrations around the cD galaxy and the second-brightest galaxy to the southeast. These two mass concentrations must merge (note also the high value of β_T mentioned above). X-ray contours show extension and perhaps a local enhancement toward the second-brightest galaxy's concentration, while another X-ray peak lies $\sim 10''$ to the northwest of the cD. The central elongation discussed above may have an extension to the northeast beyond the $1'$ radius, not associated with any apparent galaxy concentration. If the two major mass concentrations are infalling head-on, then the peak "behind" (to the northwest of) the cD may be offset from the cD by ram pressure of the gas. The elongated structure in the center, coincident with arcs and perpendicular to the merger direction, may be a shock, such as those predicted in hydrodynamic simulations (e.g., Schindler & Müller 1993; Roettiger et al. 1993). Alternatively, this structure together with its extension to the northeast may be a gas trail of an infalling galaxy group originally not associated with either of the two main subclusters. Presently, in the absence of a detailed gas temperature map in which merger shocks would be apparent, construction of such merger scenarios is highly speculative. A temperature map from *AXAF* would clarify the picture. Nevertheless, even the available X-ray imaging and optical lensing data strongly suggests that there indeed is a merger underway.

It is also possible that the absence of an X-ray peak centered on the cD is due to partial absorption by cold material, e.g., accumulated from a past cooling flow (White et al. 1992). The absorbing column should be of the order of 10^{21} cm^{-2} and higher to be noticeable in the 0.5–2 keV image. The *ROSAT* HRI data have no energy information and the angular resolution of the PSPC is insufficient to test this possibility.

Note that a merger in A2218 would imply strong temperature gradients and a likely absence of spherical symmetry, making the Hubble constant estimates using this cluster (e.g., Birkinshaw & Hughes 1994; Saunders 1997) highly uncertain.

3.3. *An Attempt of Mass Re-estimate*

Miralda-Escudé & Babul (1995) and Loeb & Mao (1994) noted that the presence of lensed images around the cD implies a mass distribution more centrally concentrated, or, equivalently, a mass inside the $20''$ lens radius greater than that derived from the hydrostatic isothermal X-ray analysis. The gas density profile they used was derived from the β-model fits to the cluster surface brightness from the *ROSAT* PSPC and *Einstein* IPC, respectively. Those fits have core radii around $1'$, consistent with the HRI result given above. Essentially, it's the absence of the radial gradient in the assumed gas density profile with $a_x = 1'$ at the lens radius of $20''$ that gives rise to the discrepancy between the X-ray and lensing mass measurements. However, it is now apparent from the better-resolution HRI data that in fact 1) the centroid of the X-ray emission is offset from the cD by about $20''$, and 2) the "core" is a blend of previously unresolved brightness peaks. As is said above, the image strongly suggests a subcluster merger and hence violent gas motions and the likely absence of hydrostatic equilibrium, the basic condition for an X-ray mass estimate. The gas turbulence proposed by Loeb & Mao essentially means the same thing.

In addition to this likely breakdown of the hydrostatic equilibrium assumption, the limited angular resolution also has a significant effect on the A2218 mass estimate. If, for example, one assumes that the head-on merger scenario is correct and the X-ray peak nearest to the cD has been displaced from the cD, then one may expect it to retain some information on the cD gravitational well (e.g., if the bulk motions are rapid enough so the gas density peak has not had enough time to disperse completely in the absence of the deep potential). For a crude estimate, we fit a simple symmetric β-model to this brightness peak excluding other parts of the image and not going too far off peak. The fit yields $a_x = 26''$ and $\beta = 0.49$. For an isothermal spherically symmetric equilibrium model, this corresponds (see e.g., Sarazin 1988) to a mass within a $20''$ radius sphere 2.6 times the mass from the "old" β-model, and to a factor of

1.4 increase in the projected mass within the cylinder of the same radius. This increase is due to the greater observed density gradient at the lensing radius, and is an underestimate if the assumed merger scenario is correct. This crude calculation illustrates the effect of insufficient angular resolution of the previous X-ray measurements on the mass at small radii around the cD.

Note that most other lensing clusters are more distant than A2218 and sufficient X-ray imaging is even more difficult to obtain. Still more problematic (practically impossible at present) is a detailed measurement of the temperature distribution for such distant clusters. Both distributions are necessary not only for an accurate hydrostatic analysis but also to judge on its applicability. First attempts at restoring the cluster mass profiles which take into account real temperature measurements (e.g., Markevitch et al. 1996; Ikebe et al. 1996; Allen et al. 1996; Loewenstein 1997; Markevitch & Vikhlinin 1997) suggest that the mass is more centrally peaked compared to that derived assuming isothermality. It is therefore possible that, together with the substructure (Bartelmann 1995) and projection effects (e.g., Daines et al. 1997) affecting the lensing analysis, inadequate modeling of gas density and temperature distributions can account for the discrepancy between lensing and X-ray mass measurements as suggested for A2218.

4. SUMMARY

The *ROSAT* HRI image of A2218 reveals complex structure in the cluster core region. One of the elongated brightness features is coincident with the bright optical gravitational arc and its counterparts. We speculate that some X-ray emission in this feature can also arise from lensing. Taking into account the detailed structure of the core can significantly increase the X-ray hydrostatic mass estimate at the lensing radius. Together with the expected mass overestimate by the lensing analysis, this can explain the previously reporetd lensing/X-ray mass discrepancy in A2218. Moreover, the image strongly suggests an ongoing subcluster merger, which makes the hydrostatic mass estimates generally inapplicable.

The author is grateful to W. Forman and A. Vikhlinin for useful discussions, comments on the manuscript and help with the HRI analysis. This work was supported by NASA grant NAG5-2611.

REFERENCES

Allen, S. W., Fabian, A. C., Kneib, J. P. 1996, MNRAS, 279, 615
Bartelmann, M. 1995, A&A, 299, 11
Birkinshaw, M., & Hughes, J. P. 1994, ApJ, 420, 33
Chartas, G., Falco, E., Forman, W., Jones, C., Schild, R., Shapiro, I. 1995, ApJ, 445, 140
Daines, S. J., Jones, C., Forman, W., & Tyson, A. 1997, ApJ, submitted
Ikebe, Y., et al. 1996, Nature, 379, 427
Le Borgne, J. F., Pello, R., & Sanahuja, B. 1992, A&AS 95, 87
Loeb, A., & Mao, S. 1994, ApJ, 435, L109
Loewenstein, M. 1997, in X-ray Imaging and Spectroscopy of Cosmic Plasmas, ed. F. Makino (Tokyo: Universal Academy), 67
Makino, N. 1996, PASJ, 48, 573
Markevitch, M., Mushotzky, R. F., Inoue, H., Yamashita, K., Furuzawa, A., & Tawara, Y. 1996, ApJ, 456, 437
Markevitch, M., & Vikhlinin, A. 1997, ApJ, submitted
Miralda-Escudé, J., & Babul, A. 1995, ApJ, 449, 18
Mushotzky, R. F., & Loewenstein, M. 1997, ApJ, in press
Navarro, J. F., Frenk, C. S., & White, S. D. M. 1995, MNRAS, 275, 270
Roettinger, K., Burns, J., & Loken, C. 1993, ApJ, 407, L53
Saunders, R. 1997, LANL preprint astro-ph/9611213
Sarazin, C. L. 1988, X-ray Emission from Clusters of Galaxies (Cambridge: Cambridge University Press)
Schindler, S., & Müller, E. 1993, A&A, 272, 137
Squires, G., Kaiser, N., Babul, A., Fahlman, G., Woods, D., Neumann, D. M., Böhringer, H. 1996, ApJ, 461, 572
White, D. 1992, PhD thesis, Univ. Cambridge
Wu, X.-P., & Fang, L.-Z. 1997, ApJ, in press

FIG. 1—*ROSAT* HRI X-ray contours overlaid on the optical image. The optical $6' \times 6'$ image is from the Digitized Sky Survey, with the central rectangular regon replaced by the *HST* image from Kneib et al. (1996). The inset in the upper right corner shows a star about $12'$ off cluster center at the same angular scale. This star was used to make a $\sim 3''$ adjustment in the relative offset of the X-ray and optical images. The HRI image is smoothed with a $\sigma = 5''$ Gaussian; contours of constant surface brightness are plotted at 0.9, 2.0, 3.2, 4.0, 4.6, 5.3, 5.8, 6.4, 7.0 $\times 10^{-6}$ counts s^{-1} $arcsec^{-2}$.